ONLINE INTERNATIONAL GEMMOLOGICAL CONFERENCE

IGC 2021

20 - 21 November 2021

www.igc-gemmology.org

Dear IGC Delegates and Observers,

On behalf of the Executive Committee of the IGC and on my personal behalf, I welcome you to the special **Online International Gemmological Seminar** organised by the Executive Committee of the IGC. As all of you know, if the Covid 19 pandemic had not disrupted our lives and schedules we would have met this year physically in Tokyo for the IGC Japan 2021. Across the Globe Corona Virus has created problems which the world never imagined possible and having personally survived the onslaught of the infection I know what it means to be just alive!

We gemmologists have always enjoyed working with gemstones - it is the thrill of the gem research that keeps us going and gives us the energy to look at the brighter side of things. So, during the last two years when the world was down, sacred and depressed, at that time many of us have diverted our focus on doing some gem research and involved our time in fruitful endeavours. It is this research work carried out during these trying times of pandemic, is being presented in this Seminar. Besides, as the new schedule for IGC Japan is 2023, it will be a great opportunity to meet everyone virtually at least!

Consideration has been given to the Time Zones to suit all the presenters, delegates and observers from Canada to New Zealand. But it is difficult. Great efforts have been put by Dr Michael S. Krzemnicki and Dr Laurent Cartier in creating the E-Copy of the Abstract Volume which will be uploaded on the IGC website.
I am sure you will appreciate all the efforts.

Once again, a Big Welcome!

All the Best.

Dr Jayshree Panjikar
Executive Secretary
IGC Executive Committee

Special IGC Online Seminar: 20-21st November 2021

Official starting time
All speakers have to join the zoom meeting 30 minutes prior to the start to check connection and solve any technical issues

11:00 PM	Sydney
08:00 PM	Hong Kong, Singapore
07:00 PM	Bangkok
05:30 PM	India, Sri Lanka
03:00 PM	Moscow (Russia)
01:00 PM	Switzerland, Germany, France...
12:00 NOON	GMT (Great Britain)
7:00 AM	New York
4:00 AM	Los Angeles

These very odd timings are due to the Time Zones in different continents. Please bear with us and be present!
Reschedule the time as per the time in your country.
All speakers **MUST** join the zoom meeting **30 minutes prior to the start of the day programme** to check connection and solve any technical issues
All speakers have to send a pdf or power point version of their talk to Michael S. Krzemnicki at the latest by **Thursday 18th November 2021** as a backup in case there is a connection problem during the session

Programme (GMT): Day 1, Saturday 20th November

12:00 Noon	**Start of Session by Zoom Convenor (Michael S. Krzemnicki), short explanation of general rules of zoom session**
12:05 to 12:15	**Welcome Address by Jayshree Panjikar (Executive Secretary of IGC Executive Committee)**
12:15	**Start of first session: Diamonds**
12:15 to 12:30	**Tian Shao & Andy Shen:** Progress on the study of Irradiated Vacancy Quenching Phosphorescence in HPHT Synthetic IIb Diamond
12:30 to 12:45	**John Chapman:** Analysis of yellow luminescing diamonds
12:45 to 13:00	**J.-P. Chalain:** Preliminary study of defocussed PL measurements
13:00 to 13:15	**Jayshree Panjikar:** Study of inclusions and types in an antique diamond ornament
13:15 to 13:30	**Stefanos Karampelas:** Gemmological and Spectroscopic Study with Mobile Instruments of The «Emeralds» from The French Crown Jewels
13:30 to 13:35	**Short break (also for additional questions, remarks)**
13:35	**Start of second session: Corundum**
13:35 to 13:50	**Supparat Promwongnan:** The chemical fingerprints of Ruby and Sapphire from Trat-Chanthaburi Gem Field, Eastern Thailand
13:50 to 14:05	**Michael S. Krzemnicki:** Zircon inclusions in unheated pink sapphires from Ilakaka, Madagascar: A Raman spectroscopic study
14:05 to 14:20	**Sudarat Saeseaw:** Effect of low-temperature heat treatment on sapphires: Inclusions and FTIR spectroscopy
14:20 to 14:35	**Pornsawat Wathanakul:** Detection of natural colour centre in yellow sapphire samples by UV-Vis-NIR excitation spectroscopy
14:35 to 14:50	**Emmanuel Fritsch:** Exploring the cause of orange luminescence in corundum
14:50 to 15:05	**Nathan Renfro:** The Micro-World of Sapphire from Secondary Sources in Montana, USA
15:05 to 15:15	**Concluding remarks of 1st Day by Zoom Convenor Michael S. Krzemnicki and Jayshree Panjikar (Executive Secretary of IGC Executive Committee)**
15:15 to 15:30	**Option: Open session for discussions/remarks**

Programme (GMT): Day 2, Sunday 21st November

12:00 Noon	**Start of Session by Zoom Convenor (Dr Hao Wang), short explanation of general rules of zoom session**
12:05 to 12:10	**Short Welcome Address by Jayshree Panjikar (Executive Secretary of IGC Executive Committee)**
12:15	**Start of third session: Other Gems**
12:15 to 12:30	**Qingchao Zhou & Andy Shen:** The Fluorescence Characteristics and Identification of Copper Diffusion-Treated Red Feldspar
12:30 to 12:45	**Lutz Nasdala:** Luminescence of gem topaz from Schneckenstein, Germany
12:45 to 13:00	**Tom Stephan:** Colour mechanisms and heat treatment of blue Nigerian gahnites
13:00 to 13:15	**Masaki Furuya:** The colouring agent of pink jadeite
13:15 to 13:30	**Claudio C. Milisenda:** Comparative characteristics of gem-quality diaspore from Afghanistan and Myanmar
13:30 to 13:45	**Hao A.O. Wang:** Cu-containing Thin Sheet Inclusion in Cu-bearing Tourmaline from Brazil
13:45 to 14:00	**Shang I (Edward) Liu:** Trapiche-Skeleton Quartz from Inner Mongolia: Crystal Morphology, Internal Features and Possible Formation
14:00 to 14:15	**Bahareh Shirdam:** Persian Turquoise; A review on the current state of Neyshabur turquoise mine, Iran
14:15 to 14:30	**Gamini Zoysa:** New giant gem corundum boulder from Sri Lanka
14:30 to 14:35	**Short break (also for additional questions, remarks)**
14:35	**Start of fourth session: Pearls**
14:35 to 14:50	**Tay Thye Sun:** Myanmar Gold-Lipped Cultured Pearls
14:50 to 15:05	**Chaoyang Chen & Andy Shen:** Progress in studying pigment evolution during the growth of freshwater cultured pearls
15:05 to 15:15	**Kentaro Emori** Analysis of Japanese Akoya Cultured Pearls using LA-ICP-MS
15:15 to 15:20	**Discussions if any Concluding remarks of Jayshree Panjikar (Executive Secretary of IGC Executive Committee)**

Are vacancies responsible for Quenching Phosphorescence in HPHT Synthetic IIb Diamond ?

Tian Shao[1], Fanglin Lyu[1], Xuewen Guo[2], Taiqiao Liu[1], Qiao Chen[1], Andy H Shen[1]

1. Gemmological Institute, China University of Geosciences, Wuhan, 430074, China
2. Center of Materials Analysis, Nanjing University, Nanjing, 210093, China

DiamondView™ is a popular apparatus in separating HPHT synthetic diamond from natural one, which essentially relies on the characteristic greenish blue phosphorescence in HPHT synthetic diamond no, you can see all varieties of emissions not just one color and its regular hour-glass poor descriptive term fluorescence distribution pattern. Yet, a recent exception had been reported, that the phosphorescence would be quenched if the diamond was irradiated under electron flux from $1.0x10^{15}$ to $1.0x10^{17}$ $e \cdot cm^{-2}$ [1]. The disappearance of phosphorescence complicates the identification process and drive up the test cost, because one had to count on other evidence to identify the HPHT synthetic diamond (e.g., detecting Ni-related defects, 883/884 nm by photoluminescence spectrometer).

The mechanism of quenching is still unknown. According to previous work [2-6] and personal communication[7], we suggested that the donor-acceptor pair recombination (DAPR) between nitrogen and boron is responsible for the greenish blue phosphorescence. Based on this speculation, if there are other defects whose energy level lies between that of donor and acceptor, it may change the phosphorescing process. In this work, we quenched the phosphorescence successfully (Fig.1) by irradiating a HPHT synthetic IIb diamond it is almost a IIa according to figure 1, thus more useful with 10 MeV electron beam under $5.6x10^{16}$ $e \cdot cm^{-2}$ flux for how long, or dose. Relying on ultraviolet-visible (UV-Vis), Fourier transform infrared (FTIR), photoluminescence (PL) and electron paramagnetic resonance (EPR) spectrometer, we checked the defects in diamond before and after the irradiation. The results manifested that the signals of neutral boron (BS^0) in FTIR and isolated neutral nitrogen (NS^0) in EPR vanished after irradiation. Instead, neutral vacancy (V^0, GR1) and negative vacancy (V^-, ND1) were detected in PL and EPR respectively. All evidences pointed to the vacancy defect GR1? which may interact with nitrogen or boron, and consequently interrupt the DAPR. Further study is in progress

Corresponding author. E-mail: shenxt@cug.edu.cn (Andy H Shen)

References

[1] Emori, K. and Koide, K. „Reduced Phosphorescence of Type II HPHT-grown synthetic diamonds after electron beam irradiation." Journal of Gemmology 36.3(2018):206-208.

[2] Watanabe, K., et al. „Phosphorescence in high-pressure synthetic diamond." Diamond and Related Materials 6.1(1997):99-106.

[3] Eaton-Magaña, S. and Lu. R. „Phosphorescence in type IIb diamonds." Diamond and Related Materials 20.7(2011):983-989.

[4] Eaton-Magaña, S. „Decay kinetics of Boron-related peak in IR absorption of natural diamond" Gems & Gemology 52.4(2016):412-413.

[5] Li, J., et al. „Direct evidence of charge transfer at boron acceptors being linked to phosphorescence in diamond" Spectroscopy and Spectral Analysis 37.6(2017):1714-1717.

[6] Shao, T., et al. „Isolated nitrogen in phosphorescence of high-temperature-high-pressure synthetic type IIb diamonds." Carbon 167(2020):888-895.

[7] Zhao, G., Personal communication.

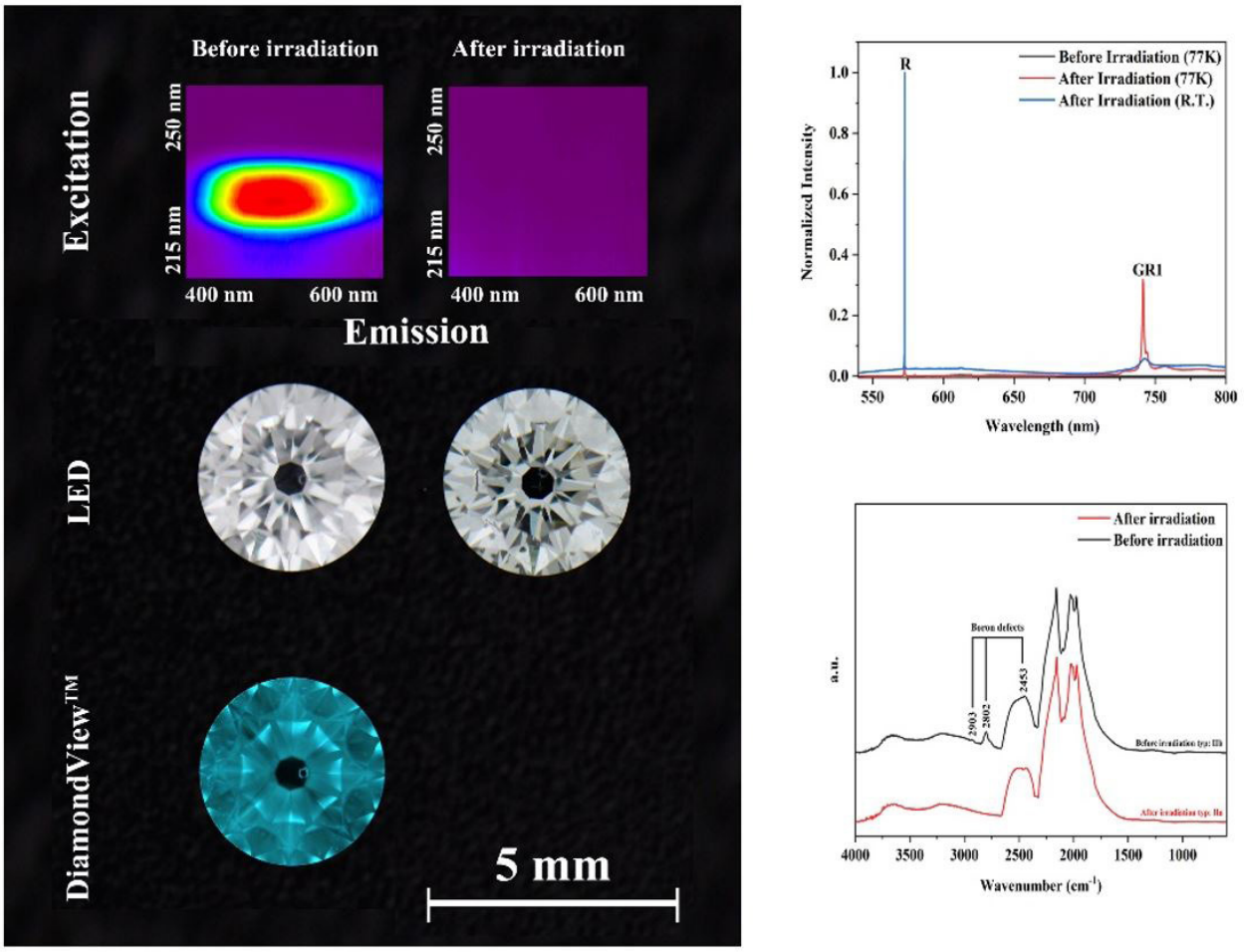

Fig.1 The PL spectrum, FTIR spectrum and the images with/without UV excitation before and after the electron irradiation treatment.

IR spectral analysis of yellow luminescing diamonds

JOHN CHAPMAN
Delta Diamond Laboratory, Perth

A collection of 45 diamonds mostly colourless, but including yellow and pink that exhibited various forms of yellow luminescence was examined. These included yellow fluorescence from LW or SW UV of which some would phosphoresce after SW exposure, and some with blue LWUV fluorescence that would exhibit yellow phosphorescence from LW. The diamonds were small in size, 1 – 2 mm and had their IR spectra recorded using a microscopic FTIR system. Some general observations were made of the spectra in the three categories, with a few notable exceptions.

Hydrogen is recognised to play a dominant role in yellow luminescence, revealed through the presence of the primary absorption peak at 3107 cm^{-1} and secondary peaks at 3142, 3180, 2781, 1432 and 1405 cm^{-1}. The strength of these peaks in combination with the A- and B-centre concentrations correlated with the luminescent behaviour. Those yellow fluorescing diamonds that did not phosphoresce generally were type IaA, with a conspicuous 3107 cm^{-1} peak along with the nearby 3142 and 3180 cm^{-1} peaks. However the spectra could not be fitted well with superimposed A and B-centre components as the 1-phonon region included a significant broad absorption that spanned 700 – 1500 cm^{-1} (see figure). This residual may be related with Ni-related S centres that are known to be associated with yellow luminescence.

The yellow fluorescing diamonds were all Type IaA (with A<300 ppm as higher concentrations would quench luminescence). Those having B-centres would exhibit dominant blue N3 emissions, with the yellow component visible as phosphorescence. The 3107 cm^{-1} peak varied significantly between these blue fluorescing samples however the 1405 cm^{-1} peak was conspicuous in each of the samples.
Yellow phosphorescence from LW UV was associated with a 1432 cm^{-1} peak that is H-related.
While the majority of yellow-luminescing diamonds exhibited the hydrogen-related centres, there were a few instances of near type II diamonds showing no discernible H-related centres.

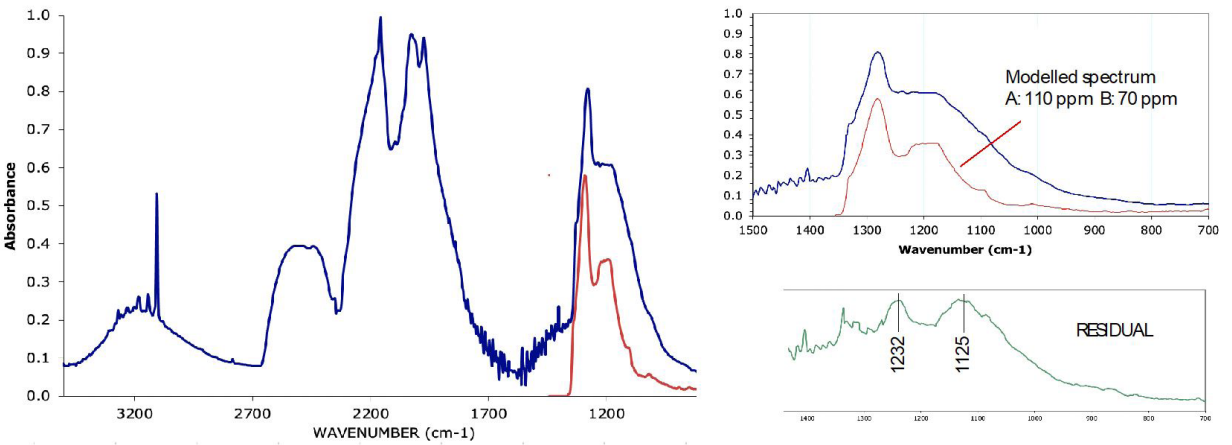

An example IR spectrum of diamond that exhibits yellow phosphorescence from SW UV.
A significant broad 1-phonon component is characteristic of these diamonds.

Preliminary study of defocused PL measurements

L. Speich, J.-P. Chalain, M.S. Krzemnicki, H. Wang, L. Phan and J. Xaysongkham
(Swiss Gemmological Institute SSEF)

In gemmology, the use of a Raman probe for inducing photoluminescence (PL) was first described by Chalain et al. 1999. Since then, PL measurements have become a common technique, for example to study optical centres in diamond (Loudin, 2017) or synthetic spinel (Krzemnicki, 2021). PL depth profile measurements, which implies defocusing the laser beam, are more exotic in gemmology but may have interesting future applications (Ardalkar et al. 2021, unpublished). Defocusing may also be used to reduce PL and Raman signals of high intensity when it is impossible to prevent detector saturation by other means.

The Swiss Gemmological Institute (SSEF) is currently conducting measurements to understand the impact of defocusing the laser spot of the Raman probe on the diamond Raman peak (DRP) as well as on different PL-active optical centres. So far, two optical centres were studied at room temperature: the N3 centre, which causes a PL peak at 415.4 nm and the SiV- centre, which produces a PL peak at 738.7 nm.

A number of measurements were performed using both green (532 nm) and violet (405nm) laser sources (for analytical parameters, see Table 1). At first, the laser beam was focussed on the table of the diamond, so that the DRP was at its maximum intensity. The distance between the diamond and the Raman probe was then varied between 6000 µm above and 6000 µm below the focal point using a z-motion stage (precision 10 µm) and a total of 35 spectra were recorded for each stone.

Figure 1 shows the behaviour of the SiV- peak in a colourless CVD synthetic diamond (reference 85822) excited by the green laser upon defocusing. Upon approaching the surface of the diamond from above, the intensity of the SiV- peak increases, reaches a maximum and then decreases inside the stone. Interestingly, the maximum was found approximately 1750 µm below the surface of the stone, not at its surface where the DRP is at its maximum intensity (not shown in Figure 1). In addition, a shoulder in the SiV- depth profile can be seen at the surface of the diamond (0 µm in Figure 1). More work is needed to examine whether the difference in behaviour between the DRP and the PL peak is due to optical phenomena or due to a real change in concentration of the SiV- defect with depth.

Laser wavelength: 405 nm		Laser wavelength: 532 nm	
Numerical aperture	0.27	Numerical aperture	0.22
Focal length	7.5 mm	Focal length	7.5 mm
Theoretical spot size	158 µm	Theoretical spot size	NA*
Depth of field	Approx. 2.2 mm	Depth of field	NA*
Analytical conditions		Analytical conditions	
Laser power	38.1 mW	Laser power	55.4 mW
Integration time	1.05 ms	Integration time	300 ms
Number of averages	1000	Number of averages	3

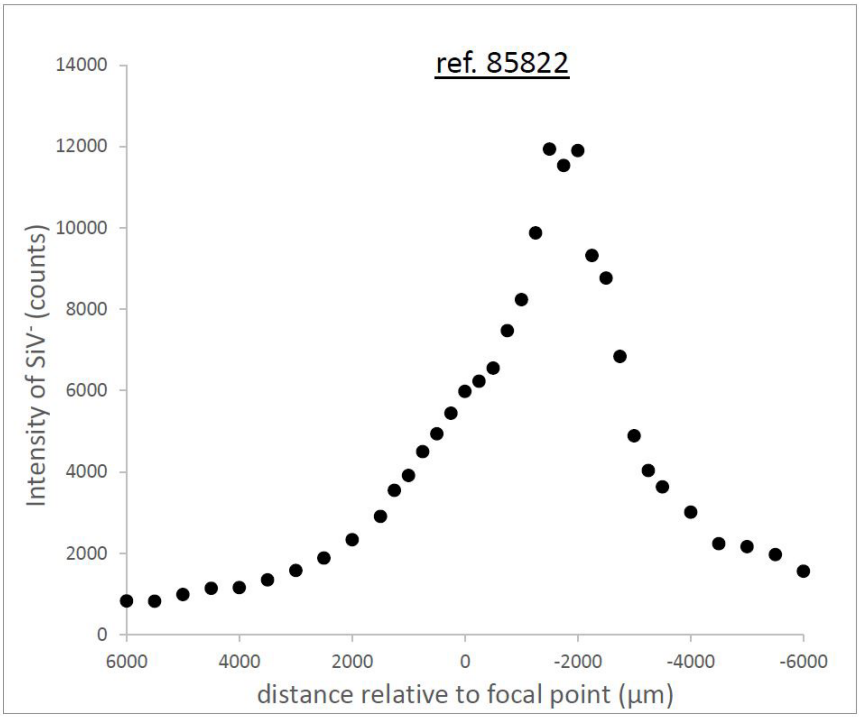

References

Ardalkar R., Salunkhe Y., Gaonkar M., Mane S., Reddy A.V.R. and Sastry M.D., 2021, Depth profile studies on natural and artificially irradiated diamonds, 2021 DeBeer's Diamond Conference

Chalain J.-P., Fritsch E. and Hänni H.A., 1999, Detection of GE-POL diamonds: a first stage, Revue de Gemmologie AFG, 138-9, p. 30-33

Krzemnicki M.S., 2021, Heated Spinel from Tajikistan, SSEF Facette 27, p. 28

Loudin, L.C., 2017, Photoluminescence Mapping of Optical Defects in HPHT Synthetic Diamond, Gems & Gemology, Vol. 53, No. 2

Study of inclusions and types in an antique diamond ornament

Jayshree Panjikar[1] and Aatish Panjikar[1]
[1]PANGEMTECH- Panjikar Gem Research & Tech Institute,
10 Sangeeta Building, Tadiwala Road, Pune 411001, India
jayshreepanjikar@gmail.com

Keywords: Characteristic inclusions, types, antique diamond ornament

The characteristic inclusions observed in an antique diamond ornament having 177 diamonds were investigated. The 177 diamonds faceted in antique rose cut and some in eight cut were of natural colour shades ranging from near colourless, pale brown, pale yellow, light green and light grey. Surface markings on polished surfaces, growth lines, graining and other features were studied and investigated wherever possible further using standard gemmological microscopes with polarising filters. These diamonds are heavily included primarily with fractures and graphite inclusions. Some of the crystal inclusions near the surface could be identified using Raman Spectroscope. Some diamonds showed some colour zoning and inclusions arranged in a pattern. When observed under the polarising microscope the crystals clearly showed some unusual interference images. Fourier-transform infrared spectroscopy indicated the diamond types to be Type IIa, IaA, IaB along with some IaA characteristics and UV-Vis spectroscopy revealed yellow diamonds as having cape lines and other diamonds displayed typical peaks for natural diamonds. UV long wave and short wave fluorescence ranged from none to blue and yellow, no diamond showed green fluorescence.

Results of these investigations have been reported

INVESTIGATIONS

The diamond ornament had 177 diamonds of which 14 stones had loose prongs and the diamonds could be removed for detailed analyses. Raman spectroscope and microscopy were used to determine the identity of some of the inclusions which consist of black colour octahedral crystals of chromite spinel, acicular crystals, elongated euhedral crystals of enstatite and black coloured material which resembles graphite type inclusions. The crystalline inclusions are randomly spread out with no orientation with respect to crystal faces indicating that the included minerals crystallized prior to the crystallization of the host diamond. Some of the diamonds have the green to light green coloured euhedral crystals of olivine (Figs 1&2) orangish red (Figs 3 & 4) coloured garnet, slightly distorted octahedral shaped crystal of spinel, blackish green diopside(Figs 5 & 6). Some of these inclusions the crystals clearly showed some unusual interference images. The 33 red beads dangling at the base of the diamond necklace were identified as natural spinel. The 10 red beads at the end of the chord on the tassels were identified as paste.

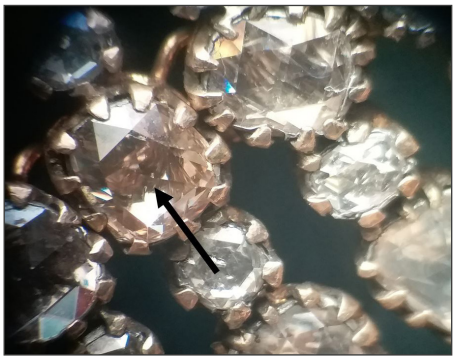

Fig 1. Inclusion of Olivine crystal

Fig2 Closeup of the olivine crystal inclusion

Fig 3 Cluster of inclusions

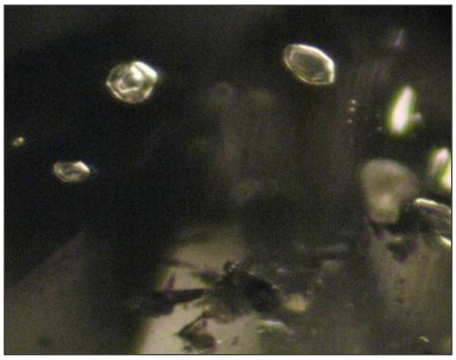

Fig 4 Closeup garnet inclusions

Fig5. Position of diopside inclusions

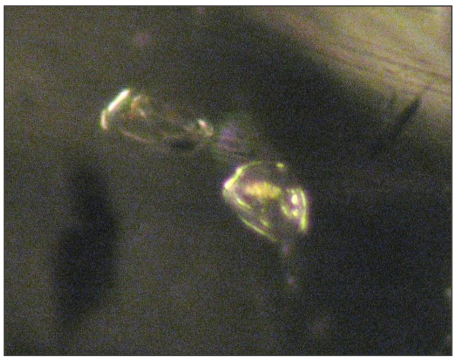

Fig 6 Close up diopside crystals

FTIR Investigation

Fourier-transform infrared spectroscopy investigation revealed that the majority of these diamonds were of type IaA having a distinctive peak at 1282cm^{-1} corresponding to A aggregate (pairs of nitrogen atoms) besides the typical absorption in the range of 1500 to 4000cm^{-1} caused by the vibronic absorption in the lattice of the diamonds which is common to all diamonds.1 The FTIR of 3 diamonds showed that they belonged to type IaB in that they showed sharp peak at 1171.4cm^{-1} along with some IaA characteristics (peak at 1282cm^{-1}). These diamonds also showed peaks due to platelet aggregates of nitrogen with extended clusters of carbon and nitrogen atoms by a sharp absorption at 1362cm^{-1}.[2] Many of the diamonds had also hydrogen impurity which was reflected in the absorption line around 3106cm^{-1}. FTIR analyses of the smaller white diamonds indicate that most of these are Type IIa.

CONCLUSION

Most of the diamonds in the old ornament had crystalline inclusions indicating them to be of natural origin. FTIR spectra clearly indicate that all diamonds are natural. Many a time old antique jewellery is sent for repair and restoration; it would be advisable to carry out a proper cataloguing using FTIR and documentation of inclusions in the old diamonds before restoration to avoid being replaced by synthetic material. Antique jewellery is being replicated today using synthetic diamonds. Present study is in this direction to help in cataloguing of old jewellery in museums and estate collections.

ACKNOWLEDGEMENTS

The authors thank Mrs. Sonali Mehta for loaning the antique diamond ornament.

References

1. G.S. Woods and A.T. Collins Infrared absorption spectra of hydrogen complexes in type I diamonds. Journal of Physics and Chemistry of Solids, Vol. 44, No 5, pp 471-475(1983)
2. G.S. Woods Platelets and Infrared absorption of type I diamonds. Proceedings of the Royal Society of London A, Vol. 407, pp219-238 (1986)

GEMMOLOGICAL AND SPECTROSCOPIC STUDY WITH MOBILE INSTRUMENTS OF THE "EMERALDS" FROM THE FRENCH CROWN JEWELS

Stefanos Karampelas[1*], Eloïse Gaillou[2], Annabelle Herreweghe[1], Farida Maouche[2], Ugo Hennebois[1], Sophie Leblan[1], Bérengère Meslin Sainte Beuve[1], Michel Lechartier[2], Didier Nectoux[2], Aurélien Delaunay[1]

[1]LFG (Laboratoire Français de Gemmologie), 30 rue de la Victoire, 75009, Paris, France
[2]MINES Paris Tech, PSL Research University, Musée de Minéralogie, 60 boulevard Saint-Michel, 75006 Paris, France
*s.karampelas@lfg.paris

Rare are the scientific studies on gemstones from the French Crown Jewels, for the good reason that most of them were sold away by the French Third Republic in 1887, to get rid of this symbol of Royalty and Empire. Some unset stones were however put aside from the big sell, and given to some French museums, including the French Natural History Museum, the Louvre, and the Paris School of Mines. Some jewels have been bought back since the late 20th by the Louvre, but mostly, the Crown Jewels are still spread out around the world.

This paper is part of an ongoing project on the study of the French Crown Jewels owned the Paris School of Mines since 1887, in collaboration with the French Gemmological Laboratory (LFG). As this National Treasure is security sensitive, the project had to be conducted on site at the MINES Paristech Mineralogy Museum, using portable analytical instruments. In this first study, we are presenting the results acquired on some green coloured gems that used to be part of the coronation Crown of Napoleon III. Before it was melted down in 1887, the crown was adorned with 8 relatively large emeralds weighing from 14.5 to 23.7 carats as well as 8 relatively large diamonds weighing from 17 to 26.3 carats. Fifty smaller emeralds were also adorning the crown: 34 at the top and 16 at the bottom of it. These 50 smaller emeralds were part of the donation to the Paris School of Mines in 1887. Today, 33 out of the 34 samples from the top of the crown as well as 12 out of 16 samples from the bottom are catalogued in the Museum's collection.

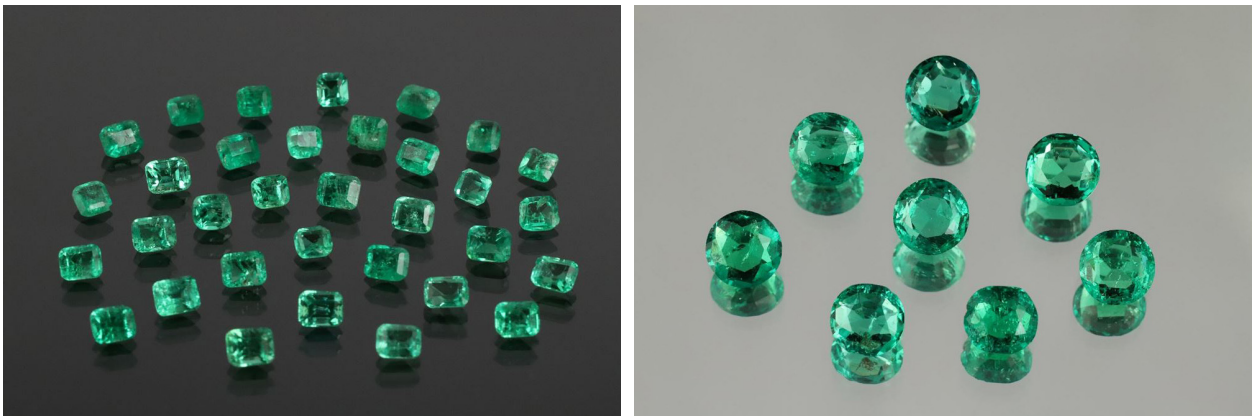

Fig 1. Emeralds originally set in the coronation Crown of Napoleon III, most likely from Colombia.
Left: 33 smaller emeralds weighing from 0.18 to 0.41 carats (ENSMP 69880).
Right: 8 larger emeralds weighing from 0.85 to 1.34 ct (ENSMP 69866) © Musée de Minéralogie MINES ParisTech / Eloïse Gaillou.

All 45 green stones were observed macroscopically and under optical microscope (up to 80x). Raman spectra were carried out using a mobile Raman spectrometer with a 532 nm excitation wavelength, Vis-NIR spectra were acquired from 365 to 1000 nm using an integrating sphere and FTIR spectra from 400 to 8000 cm^{-1} using a DRIFT accessory. 33 of the studied gems are faceted in octagonal/step cut weighing from 0.18 to 0.41 carats (Figure 1) and 12 samples are in round/brilliant cut (with one oval shaped) weighing from 0.70 to 1.34 carats. All 33 octagonal samples and 8 of the roundish shaped samples (see again Figure 1) present Raman spectra characteristic of beryl (Bersani et al., 2014). The other 4 roundish shaped samples present large bands in the Raman spectra often observed on some glasses (Robinet et al., 2006). Natural multiphase inclusions, colour zonation and in some cases "gota de aceite" structures are observed in all 41 beryl samples. On the other hand, air bubbles are observed in the 4 glass samples. Vis-NIR spectra of the 41 emerald samples display absorption bands related to chromium and vanadium; no absorption bands related to iron were observed (Figure 2; Wood and Nassau, 1968). The 4 glasses present bands linked to iron (Carl et al., 2007). FTIR spectra of the 41 emeralds present bands linked with low alkali content emeralds and the four glasses some large bands.

With the combination of spectroscopic and microscopic methods, the 41 green gems originally set in the coronation Crown of Napoleon III are identified as natural emeralds with Colombia as their most probable source (Saeseaw et al., 2019). The other 4 stones are identified as green artificial glasses. It is currently still unknown whether these 4 glass stones were set from the beginning in the crown or exchanged at a later stage.

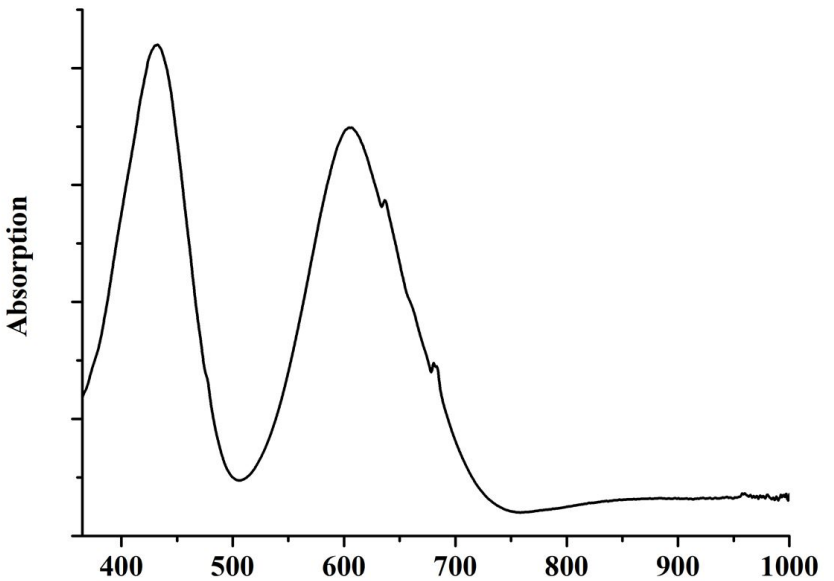

Figure 2: Vis-NIR absorption spectrum from 365 to 1000 nm of an emerald originally set in the coronation Crown of Napoleon III displaying bands related to chromium and vanadium; no absorption bands related to iron were observed.

References

D. Bersani, G. Azzi, E. Lambruschi, G. Barone, P. Mazzoleni, S. Raneri, U. Longobardo, P. P. Lottici (2014). Characterization of emeralds by micro-Raman spectroscopy. J Raman Spectrosc, Vol. 45, No. 11-12, pp. 1293-1300.

R. Carl, S. Gerlach, C. Rüssel (2007). The effect of composition on UV-Vis-NIR spectra of iron doped glasses in the systems $Na_2O/MgO/SiO_2$ and $Na_2O/MgO/Al_2O_3/SiO_2$. J Non-Cryst Solids. Vol. 353, No. 3, pp. 244-249.

L. Robinet, C. Coupry, K. Eremin, C. Hall (2006). The use of Raman spectrometry to predict the stability of historic glasses. J Raman Spectrosc, Vol. 37, No. 7, pp. 789-797.

S. Saeseaw, N. D. Renfro, A. C. Palke, Z. Sun, S. F. McClure (2019). Gems Gemol, Vol. 55, No. 4, pp. 614-646.

D. L. Wood, K. Nassau (1968). The characterization of beryl and emerald by visible and infrared absorption spectroscopy. Am Mineral, Vol. 53, No. 5-6, pp. 777-800.

The chemical fingerprints of ruby and sapphire from Trat-Chanthaburi Gem Field, Eastern Thailand

Supparat Promwongnan[1], Chakkaphan Sutthirat[1,2], Visut Pisutha-Arnond[1], Wilawan Atichat[1], Thanong Leelawathanasuk1

[1]The Gem and Jewelry Institute of Thailand, psupparat@git.or.th
[2]Department of geology department, faculty of science, Chulalongkorn university

The gem corundum deposits in Thailand, including those in the Trat-Chanthaburi gem field, are associated with late Cenozoic alkaline basalts within the extensional tectonic environments. According to several in-depth studies (Coenraads, 1992; Khamloet et al., 2014; Promwongnan and Sutthirat, 2019; Saminpanya and Sutherland, 2011; Sutherland et al., 1998), rubies and blue-green-yellow (BGY) sapphires are believed to derive from two different modes of origin prior to being carried upward onto the surface by the Cenozoic alkaline basaltic magmas. The rubies were originated from a mafic granulite, a high-grade metamorphic rock formed in the upper mantle. The BGY sapphires, on the other hand, were derived from a magmatic origin which appeared to have crystallized from a highly evolved syenitic melt and/or its metasomatized product in the middle or lower crust. Dating from the 1890s, most rubies and sapphires from Trat-Chanthaburi gem field were mined out of alluvial deposits of those corundum bearing basalts with primitive tools before productive mechanized methods.

A geographic origin of a gem corundum is, often in the trade, considered a significant factor influencing the stone valuation, particularly of those from some eminent localities. An origin of a gem corundum could be distinguished by using locality-specific inclusions, characteristic absorption spectra, and trace element signatures. In fact, the trace element constitutes are commonly used as a leading and powerful guidance for gem provenance determination. Among a number of methods being used to analyze the stone´s chemical nature, the EDXRF is an equipment that is widely employed in the gem labs to establish the chemical fingerprint of gemstones as it is non-destructive, quick and easy to use, and cost-effective.
Samples of ruby (in the absence of sapphire) from the Bo Rai deposit in Trat Province and ruby plus sapphire from Bo Welu deposit in Chanthaburi Province were collected and analyzed by the EDXRF method for major and trace element compositions.

The chemical fingerprint of rubies from both areas revealed high contents of Fe and Cr (0.35-1.26 wt% Fe_2O_3, 0.06-0.94 wt% Cr_2O_3), intermediate Ti content (0.01-0.67 wt% TiO_2) and low V and Ga concentrations (up to 0.03 wt% Ga_2O_3, up to 0.04 wt% V_2O_5). Moreover, Bo Welu rubies appear to have V, Cr and Fe contents lower than those of Bo Rai rubies.

When compared with rubies from other basalt-related localities such as Cambodia (Pailin, Kao Tawow, Bo Yakha) and Kenya (Simba and Baringo), the Thai and Cambodian rubies do share similar trace element signatures and they are relatively rich in Cr, and poor in V and Ga with Cr_2O_3/Ga_2O_3 <100 indicating that they were derived from an ultramafic (upper mantle) source. These deposits, however, have higher Fe contents and lower V contents than those from Kenya (Figure1).

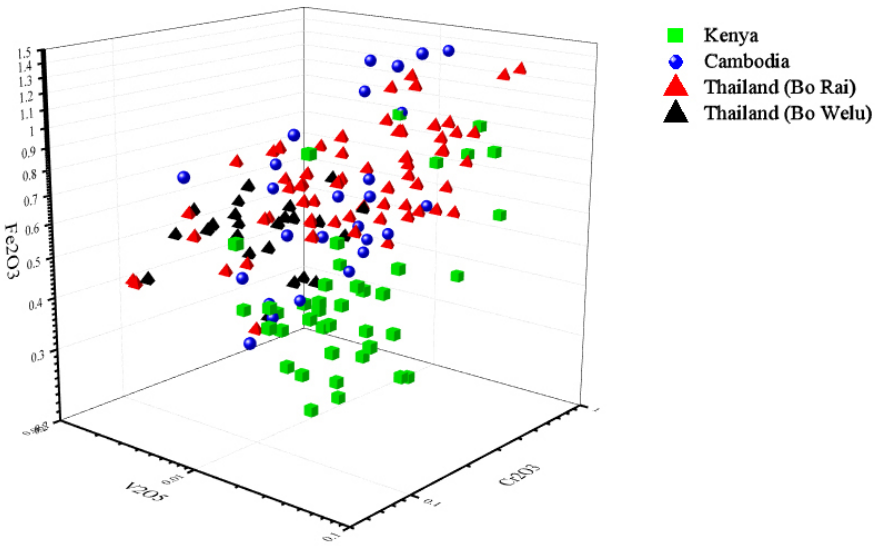

Figure 1. 3D plot of Cr2O3-V2O5-Fe2O3 contents of basalt-related rubies from Thailand (Bo Welu, Bo Rai), Cambodia, and Kenya.

The chemical fingerprint of blue-green (BG) sapphire from Bo Welu deposit yields noticeable Fe enrichment (0. 45-1.38 wt% Fe_2O_3), low Ga (0.01-0.05 wt% Ga_2O_3) and Ti (0.01-0.09 wt%TiO_2) and relatively poor Cr (up to 0.01wt% Cr_2O_3). By comparison among the basaltic BG sapphires found in the country, Bo Welu sapphires have somewhat higher Ga and lower V contents than the sapphires from other gem deposits in Thailand, i.e., Phrae, Kanchanaburi (Bo Ploi), Chanthaburi (Khao Ploi Wuen, Khao Wua and Tokphrom) (Figure 2). In addition, the Bo Welu sapphire has Fe/Ga ratio lower than the sapphires from Khao Ploi Wuen and Khao Wua of the same gem field (Figure 3). Thus, the Bo Welu sapphires could have been crystallized from an extremely evolved syenitic magma which was very poor in Cr and quite rich in Ga with Cr_2O_3/Ga_2O_3 <1.

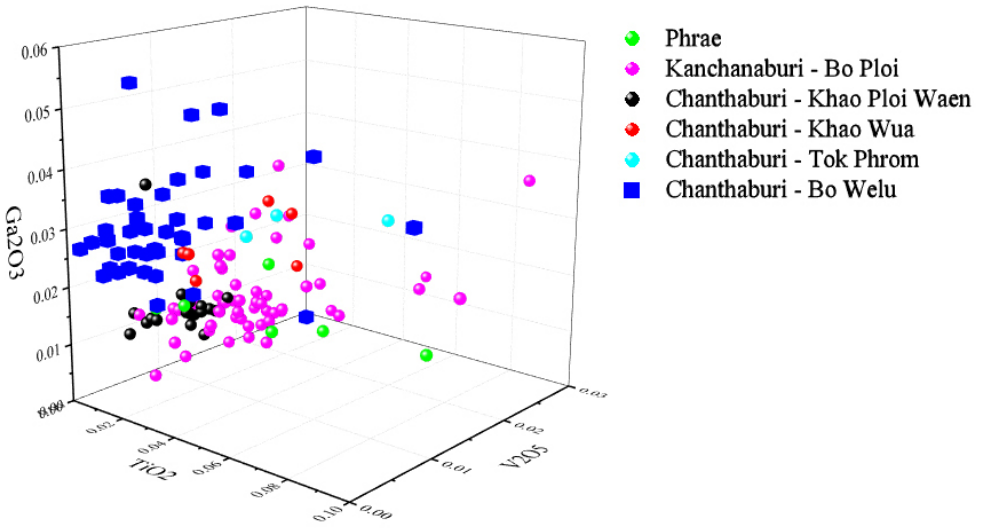

Figure 2. 3D-plot of V_2O_5-TiO_2-Ga_2O_3 contents of basaltic blue-green sapphires from Bo Welu and other gem deposits in Thailand.

In comparison with some basalt-related BG sapphires around the world (i.e., Australia, Madagascar, Nigeria, Cambodia, and Laos), the Bo Welu sapphires have Fe/Ti ratio higher than the basaltic sapphires from Nigeria, Cambodia, and Laos (Figure 4) In addition, the Bo Welu sapphires appear to have lower V content than the basaltic sapphires from the other deposits.

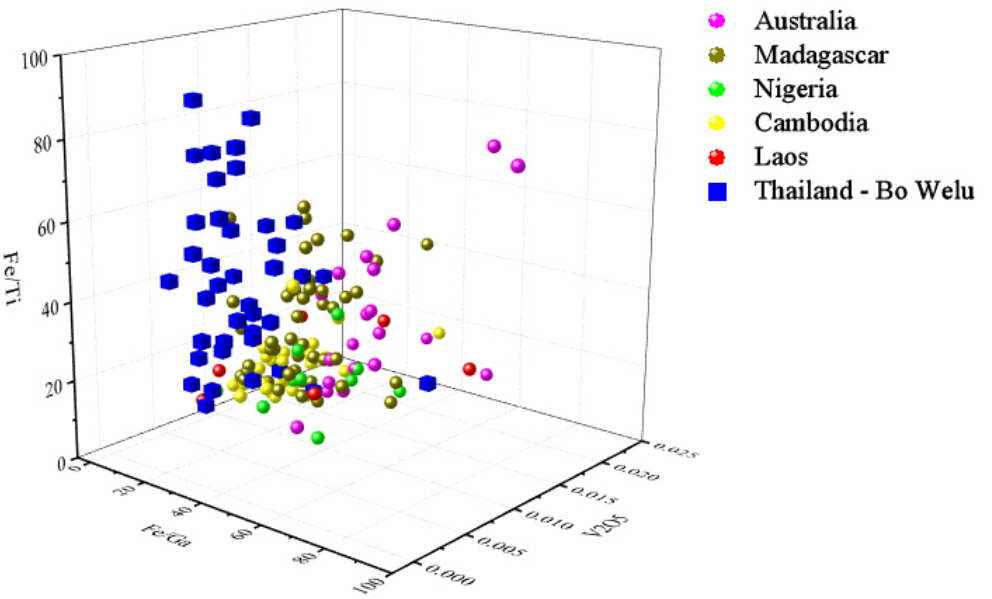

Figure 4. 3-plot of V_2O_5 content-(Fe/Ga)-(Fe/Ti) ratios of Bo Welu sapphires and some basaltic sapphires from other gem fields around the world, by EDXRF analysis.

References

Coenraads, R.R., 1992. Surface features on natural rubies and sapphires derived from volcanic provinces. Journal of Gemmology, 23(3), 151-160.

Khamloet, P., Pisutha-Arnond, V. and Sutthirat, C., 2014. Mineral inclusions in sapphire from the basalt related deposit in Bo Phloi, Kanchanaburi, Western Thailand: indication of their genesis. Russian Geology and Geophysics, 55(9), 1087-1102.

Promwongnan, S. and Sutthirat, C., 2019. Mineral inclusions in ruby and sapphire from Bo Welu gem deposit in Chanthaburi Province, Eastern Thailand. Gems & Gemology, 55(3), 354–369.

Saminpanya, S. and Sutherland, F.L., 2011. Different origins of Thai area sapphire and ruby, derived from mineral inclusions and co-existing minerals. European Journal of Mineralogy, 23(4), 683-694.

Sutherland, F.L., Hoskin, P.W., Fanning, C.M. and Coenraads, R.R., 1998. Models of corundum origin from alkali basaltic terrains: a reappraisal. Mineralogy and Petrology, 133(4), 356-372.

Zircon inclusions in unheated pink sapphires from Ilakaka, Madagascar: A Raman spectroscopic study

M.S. Krzemnicki, P. Lefèvre, W. Zhou, H.A.O. Wang
Swiss Gemmological Institute SSEF
gemlab@ssef.ch

Since its discovery in 1998, the secondary gem deposit of Ilakaka, southwestern Madagascar has produced a large number of outstanding stones for the gem trade, notably sapphires and fancy sapphires in a wide range of colours (Milisenda et al. 2001). Until today, pink sapphires from Ilakaka are found in great numbers in the trade, often characterised by an outstanding quality and a pastel pink to vivid pink ("hot pink") colour.

Interestingly, pink sapphires from Ilakaka commonly contain numerous rounded zircon inclusions, sometimes even clustered in aggregates (Figure 1). Zircon is found in corundum from many different geological settings and geographic origins and may provide crucial information for gem testing, both, regarding heat treatment (Wang et al. 2006, Krzemnicki 2010, Saeseaw et al. 2020) and origin determination (Xu & Krzemnicki 2021).

The Raman analysis of zircon inclusions in pink sapphires from Ilakaka (Madagascar) is widely used in gem labs as a routine test as it may provide supporting analytical evidence of a heat treatment. In this study, we focus on Raman spectra of zircon inclusions in unheated pink to purplish pink sapphires from Ilakaka to better characterise and understand the range and variability of the SiO_4-related bandwidths. More than 100 zircon inclusions in 28 samples (rough and cut) from the SSEF research collection were analysed using an InVia Renishaw Raman microprobe coupled with a 514 nm argon-ion laser. In accordance with literature (Nasdala et al. 1995, Wang et al. 2006, Saeseaw et al. 2020) we focussed on the main Raman peak υ3 (SiO_4 anti-symmetrical stretching mode) of zircon at about 1010 cm^{-1} as a measure of its crystallinity (or degree of metamictization). From these spectra we determined the υ3 bandwidth (FWHM: Full-Width-Half-Maximum) by fitting into a software-integrated Gaussian-Lorentzian function after baseline correction.

Our results of all analysed zircon inclusions in unheated samples show a large variation of υ3 peak position and bandwidth not only in different pink to purple sapphires, but even in neighbouring zircon inclusions within the same specimen (Figure 2). Interestingly, we also found peak variations when measuring several different positions of selected single zircon inclusions. The FWHM of υ3 in our unheated samples range between 7.5 to 17.6 cm^{-1}, with a median value of below 10. Similar results have been described by Wanthanachaisaeng (2006, 2007). Our analyses in unheated rough and cut pink sapphires from Ilakaka, however, reveal bandwidth values distinctly lower than those reported by Wang et al. (2006) and Saeseaw et al. (2020) in their samples. Our results show, that heat treatment detection of pink sapphires from Madagascar based on Raman spectra of zircon inclusions alone needs to be applied cautiously to avoid misinterpretations.

Figure 1: Pink sapphire of 7.9 ct from Ilakaka, Madagascar and photomicrograph of zircon inclusions (magnification 50x).

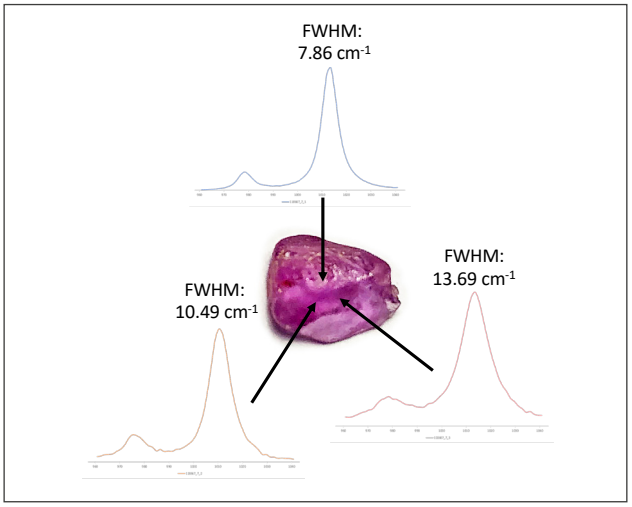

Figure 2: Variability of the bandwidth (FWHM) of the main zircon Raman peak at about 1010 cm^{-1} in three different zircon inclusions in an unheated rough pink sapphire from Ilakaka, Madagascar.

References

Krzemnicki M.S. (2010) How to get the "blues" out of the pink: Detection of low-temperature heating of pink sapphires. SSEF Facette, No. 17, p 12

Milisenda, C.C., Henn, U., and Henn, J. (2001). New gemstone occurrences in the south-west of Madagascar. Journal of Gemmology, 27(7), 385-94

Nasdala L., Irmer G., Wolf D. (1995) The degree of metamictization in zircon: A Raman spectroscopic study. European Journal of Mineralogy, 7(3), 471-478

Saeseaw S., Khowpong C., & Vertriest W. (2020). Low-temperature heat treatment of pink sapphires from Ilakaka, Madagascar. Gems & Gemology, 56(4), 448-457

Wang W., Scarratt K., Emmett J.L., Breeding C.M., Douthit T.R. (2006) The effects of heat treatment on zircon inclusions in Madagascar sapphires. Gems & Gemology, 42(2), 134-150

Wanthanachaisaeng, B., Häger, T., Hofmeister, W., and Nasdal, L. (2006). Raman- und fluoreszenz-spexktroskopische Eigenschaften von Zirkon-Einschlüssen in chrom-haltigen Korundum aus Ilakaka und deren Veränderung durch Hitzebehandlung. Zeitschr. Deutschen Gemmol. Gesell., 55, 119-132.

Wanthanachaisaeng B. (2007). The influence of heat treatment on the phase relations in mineral growth systems. PhD thesis, J. Gutenberg University Mainz, Germany, 79 pp.

Xu W., Krzemnicki M.S. (2021). Raman spectroscopic investigation of zircon in gem-quality sapphire: Application in origin determination. Journal of Raman Spectroscopy, 52 (5), 1011–1021

Effect of low-temperature heat treatment on sapphires: Inclusions and FTIR spectroscopy

Sudarat Saeseaw[1], Ungkhana Atikarnsakul[1], Wasura Soonthorntantikul[1]

[1]GIA Gemological Institute of America, Bangkok, Thailand
ssaeseaw@gia.edu

For many centuries, heat treatment is applied on corundum to improve their colour and/or clarity. The low temperature heat treatment has been carried out for a thousand years to lighten the blue coloration in dark blue sapphires and remove/reduce blue patches in ruby and pink sapphires to obtain the desirable colours. Detecting this low temperature treatment is challenging to gemmological laboratories due to minor changes in microscopic inclusions. Therefore, analytical instrument such as infrared spectroscopy is a crucial tool that can be useful for heat treatment detection.

FTIR is considered a useful aid in heat treatment identification in corundum. The most interested feature is in mid-infrared region between 1900 to 4000 cm^{-1} which contains the structural OH stretching in corundum. The most common features are the 3309-series (3309, 3232, 3185 cm^{-1}) that often found in heated low-iron metamorphic blue sapphires (Hughes, 2019), heated Mozambique rubies (Saeseaw, 2018), and in flame-fusion synthetic sapphires/rubies (Smith, 1995). The 3161-series (3161, 3242 and 3355 cm^{-1}) that reported to OH- associated with Mg^{2+} that excess from the charge compensation by Si^{4+} and Ti^{4+} in the acceptor dominated stones. (Smith, 2006) which occurs commonly in natural yellow to orange and padparadscha sapphires from metamorphic environment. The 3000-series, typically known as 'Punsiri series', is characteristic of the "Punsiri" high-temperature heat treatment in low-Fe blue sapphires and traditionally used as indicative of heat treatment. This IR pattern consists of a wide band centered at around 3010-3070 cm^{-1} along with medium width peaks at 3195, 2625, 2463 and 2415 cm^{-1}. Recently, it has been reported that the 3000 cm^{-1} broad band series is not induced by heat treatment only but also may occur naturally. This characteristic IR feature is previously seen in natural unheated yellow sapphires from basalt-related deposits, including Thailand and Australia.

In this study, authors observed a colour appearance, internal features and FTIR before and after heat treatment at varied heating conditions. There were three sets of experiment including

a) Pink sapphires. Eleven (11) samples from Ilakaka, Madagascar that contained a single peak of 3309 cm^{-1}, were selected for heated treatment in air at 800 °C for 160 minutes.
b) Basalt blue sapphires. Four (4) samples that revealed the 3309-series, were selected and heated in air at 500, 700, 900, 1100 and 1300 °C for 7 hours.
c) Yellow sapphires. Twelve (12) samples from Sri Lanka and Madagascar that initially displayed 3161 cm^{-1} peak, were selected for heat treatment in air at 500, 700, 900 and 1050°C for a fixed duration of 6 hours.

Results and discussion

a) Pink sapphires. The results showed a blue component in the pink sapphires was reduced and the samples were purer pink. Only a few microscopic features such as mica and monazite crystals had developed tension fractures. All samples showed a decreased 3309 cm^{-1} peak while only 9 Madagascan samples had developed a peak at 3232 cm–1 and none of a peak at 3185 cm^{-1} detected (Figure 1). This result is also observed in low temperature heated rubies from Mozambique.

b) Basalt blue sapphires. The results indicated a negligible change or a slight lightening of the blue colour after treatment at 700°C, while an obvious lightening of the blue colour resulted from heating at 900°C and 1050°C. Some solid inclusions, iron stains, and partially healed fractures showed signs of alteration during the heating experiments, while needles and minute particles did not show any signs of change. FTIR showed a reduction of 3309 cm^{-1} peak and raise in 3232 cm^{-1} after heating at 700°C and 900°C (Figure 2). However, some samples that initially showed a relatively intense 3232 cm^{-1} peak in the series before treatment exhibited a more intense 3309 cm^{-1} peak and a less intense 3232 cm^{-1} peak post-treatment.

c) Yellow sapphires. The results indicated no change in colour appearance when heated at 500 and 700 C, samples showed stronger yellow zones when heated at 900 and 1050 C. Only few internal features affect to heat treatment such as crystals that developed tension fractures and no alteration in minute particles. Interstingly, FTIR exhibited a reduction of 3161 cm^{-1} peak when heating at 900 C and sometimes start developed a 3000 series bands with a broad band at 2625 cm^{-1} when heated at 900 C and above in air (Figure 3).

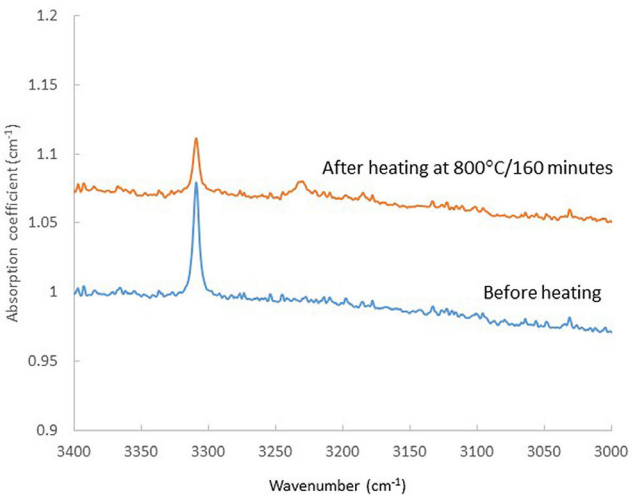

Sample no.	Before heating	After heating	
	3309 cm^{-1}	3309 cm^{-1}	3232 cm^{-1}
PS01	0.04	N/A	N/A
PS02	0.04	0.02	0.005
PS03	0.07	0.04	0.01
PS04	0.07	0.04	0.01
PS05	0.04	0.02	N/A
PS06	0.05	0.02	0.01
PS07	0.05	0.03	0.01
PS08	0.06	0.03	0.01
PS09	0.06	0.03	0.01
PS10	0.06	0.03	0.01
PS11	0.04	0.01	0.005

Figure 1. (Left) Comparison FTIR spectra before (blue) and after (orange) heat treatment (Right) comparison between peak heights before and after heat treatment at 800°C for 160 minutes on an unoriented pink sapphire from Madagascar.

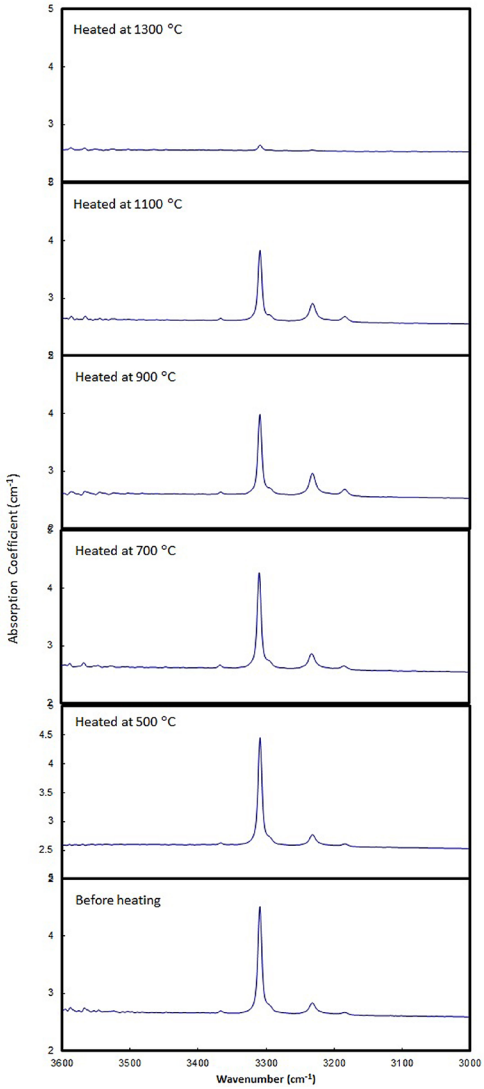

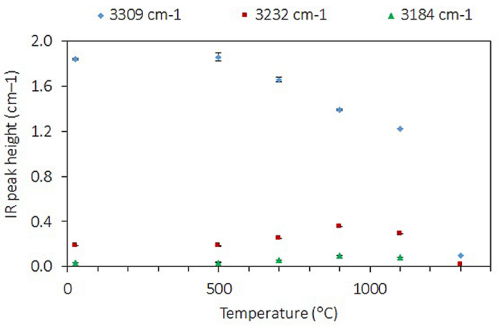

Figure 2. (Left) Representative of FTIR spectra on Camodia blue sapphire before and after heating (Right) Plot of FTIR peak height at 3309, 3232 and 3185 cm^{-1} at different temperatures between 500 and 1300°C for 7 hours.

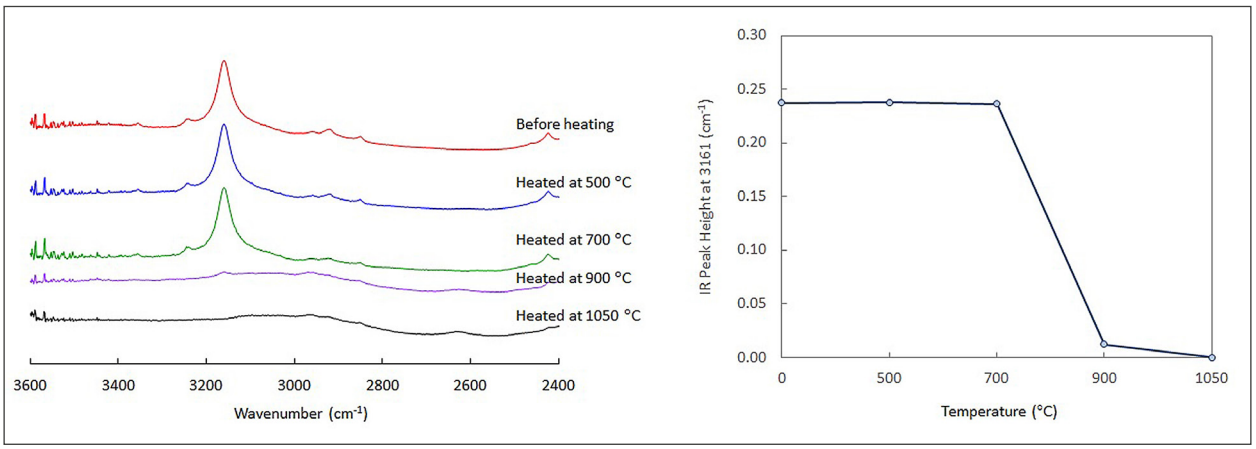

Figure 3. (Left) Representative of FTIR spectra on Sri Lanka yellow sapphire before and after heating (Right) Plot of FTIR peak height at 3161 cm^{-1} at different temperatures between 500 and 1050°C for 6 hours.

The results show that FTIR can be useful to detect low temperature treatment in certain types of sapphires. The combination of a 3000-series with 2625 cm^{-1} peak in low Fe yellow sapphire is a strong indicator heat treatment. This is very helpful, especially when stones are clean. However, a presence or absence of 3161 cm^{-1} cannot be used as indication of unheating since there is no relation of 3161 cm^{-1} intesity between before and after heat treatment. A presence of 3309-series in pink sapphires indicate of heat treatment. Based on our experiments, FTIR spectroscopy of basaltic blue sapphires is more complicated and criteria to detect heat treatment are yet to be discovered.

References

Atikarnsakul, U., Emmett, J.L, 2021. Heat treatment effects to the behavior of 3161 cm^{-1} feature in low iron metamorphic yellow sapphires. Gems & Gemology, 58.

Beran, A., Rossman, G.R., 2006. OH in naturally occurring corundum. European Journal of Mineralogy, 18, 441-447.

Hughes, R.W., Emmett, J.L., Dubinsky, E.V., Scarratt, K., 2017. Ruby & Sapphire: a gemologist's guide. RWH publishing/ Lotus publishing, Thailand, pp. 146-149.

Hughes, E.B., Perkins, R., 2019. Madagascar Sapphire: Low-Temperature Heat Treatment Experiments. Gems and Gemology, 55 (1), 184-197.

Saeseaw, S., Konsomart, B., Atikarnsakul, U., Khowpong, C., Vertriest, W., Soonthorntantikul, W., 2018. Update on "low-temperature" heat treatment of Mozambican ruby: A focus on inclusions and FTIR spectroscopy. https://www. gia. edu/doc/low_HT_Moz_report.pdf.

Sangsawong, S., Pardieu, V., Raynaud, V., Engniwat, S., 2016. "Punsiri"-type FTIR spectral features in natural yellow sapphires. Gems and Gemology, 52 (3), 325-327.

Smith, C.P., 1995. A contribution to understanding the infrared spectra of rubies from Mong Hsu, Myanmar. Journal of Gemmology, 24 (5), 321-335.

Smith, C.P., 2006. Infrared spectra of gem corundum. Gems & Gemology, 42 (3), 92-93.

Detection of natural colour centre in yellow sapphire samples by UV-Vis-NIR excitation spectroscopy

Wiwat Wongkokua[1], Natthapong Monarumit[2], Thanapong Lhuaamporn[3], Gamini Zoysa[4] and Pornsawat Wathanakul[2]

[1] Department of Physics, [2] Department of Earth Sciences, Faculty of Science, Kasetsart University, Bangkok, Thailand;
[3] The Gem and Jewelry Institute of Thailand; [4] CGS, Colombo, Sri Lanka
pwathanakul2@gmail.com

The UV-Vis-NIR excitation spectroscopy can be used to help reveal the causes of yellow coloration in sapphires. Monarumit, et al. 2020 reported excitations at 423 nm, 457 nm, 487 nm and 553 nm and emissions at 609 nm and 841 nm in Be-diffused yellow sapphire samples by using this technique; those excitations and emissions are due to the existences of mixed Fe^{3+}-Be^{2+} electron donor energy states in the energy band gap (EBG) of the samples, promoting the yellow coloration due to colour centre induced by Be. The experiment on detection of natural yellow colour centre (NYCC) has been conducted on eleven yellow sapphire samples shipped directly from Sri Lanka, which normally contain Mg as one of trace elements. The representative spectrum provided by one of those samples reveals the NYCC excitations centred at 406 nm, 459 nm and 485 nm by using fine multipeak fitting software (Figure 1). The excitations are due to the mutual Fe^{3+}-Mg^{2+} electron donor states in the EBG, providing the yellow coloration caused by the natural colour centre in the representative sapphire sample.

The portable UV-Vis-NIR excitation spectrometer (tungsten lamp, spectrum range 275 nm to 1100 nm, CCD detector, with an integrating sphere) can help support gemmologists in utilising the lower cost instrumentation to reveal the causes of coloration in sapphire samples. The presentation includes the update on causes of yellow coloration in sapphires, in which the energy band theory better elaborates the explanations.

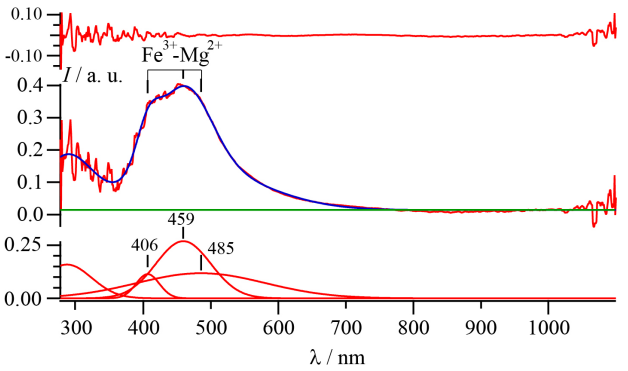

Figure 1: The representative UV-Vis-NIR excitation spectrum of a natural yellow sapphire from Sri Lanka (blue), with fine multipeak fitting showing excitations at 406 nm, 459 nm and 485 nm (bottom) due to the mutual Fe^{3+}-Mg^{2+} electron donor states in the energy band gap of the sample.

References

Monarumit, N., Lhuaamporn, T., Sakkaravej, S., Wathanakul, P., Wongkokua, W., 2020. The color center of beryllium-treated yellow sapphires. Journal of Physics Communications. 4(10), 105018

Exploring the cause of orange luminescence in corundum

Maxence Vigier[1], Emmanuel Fritsch[1], Olivier Segura[2]

[1]Université de Nantes, CNRS, Institut des Matériaux Jean Rouxel, IMN, F-44000 Nantes, France
(*correspondance: emmanuel.fritsch@cnrs-imn.fr)
[2]l'Ecole des Arts Joailliers, 22 Place Vendôme - 75001 Paris – France
(Olivier.Segura@vancleefarpels.com)

Keywords: orange luminescence, corundum, fluorescence, F center, emission

The cause of orange luminescence in corundum is unknown. We documented many aspects of this emission: emission, excitation, luminescence decay, relation to defects, covering natural, treated and synthetic samples about 50 in total. Here, we present only the first two sets of data. Figure 1 demonstrates that in the emission spectra the major feature is a broad band around 620 nm which is responsible for the orange luminescence (Vigier et al, 2021). Indeed, the eye perceives the orange part of this feature far more efficiently than the red part. The broad band is made more apparent when the emission spectra are corrected for Cr^{3+} emission, also present in many of the gems.

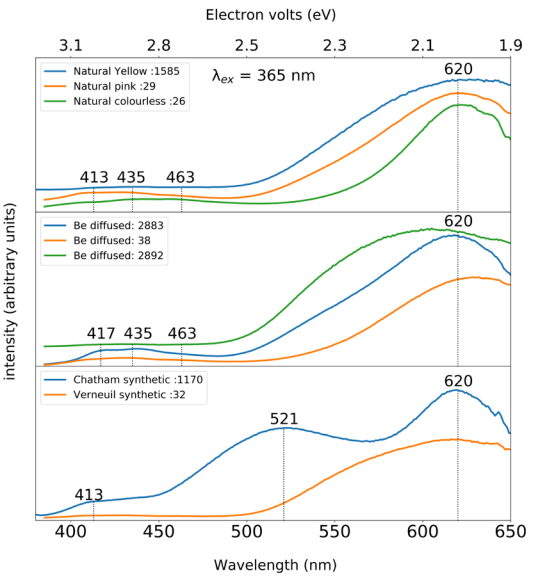

Figure 1: Corrected emission spectra of our orange luminescent samples sorted by type of corundum, respectively natural, Be diffused and synthetic. The orange is associated with the central emission band at 620 nm. Additional luminescence is measured in other spectral ranges: green (521 nm, one sample) and violet-blue (at approximately 410, 420 or 440 nm for ex, seen in several samples).

Excitation spectra in figure 2 demonstrate the absorptions providing energy for the emission. They are the first insight into the origin of the luminescence.

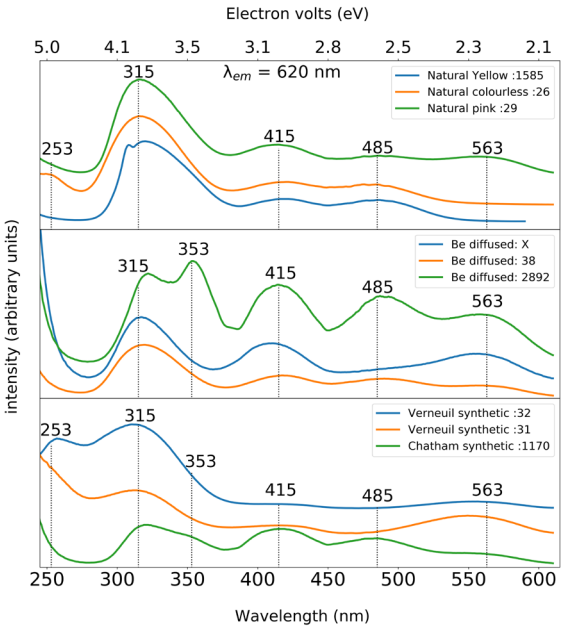

Figure 2: Comparison of the excitation spectra associated with the orange luminescence band at 620 nm, carried out at room temperature, on our samples, natural, chemically treated and synthetic. The spectra are generally all similar and contain the same set of bands centred at 315, 353, 415 and 485 nm. Additional bands at 253 and 563 nm were recorded occasionally, without an obvious link to the nature of the material

According to the literature (see e.g., Atobe et al, 1985), reviewed in Vigier (2021), these bands are all related to F centers. These represent oxygen vacancies, that is the absence of an oxygen atom at its intended place in the crystal structure, one of the most common defects in oxides. They may have various charges and may be trapped at Mg^{2+} or other divalent ions. The 253 nm arises from a F-center bound to Mg, and that at 315 nm, to a F_2^+ center bound to two Mg. An F_2^+ center bound to single Mg is the source of the 353 nm feature. The band around 415 nm is said to arise from a F_2^{2+} centre bound to 2 Mg, while that at 485 nm, to a F center bound to a Mg (like the 253 nm feature). Finally, the 563 nm has been linked to a F_2^+ (Atobe et al. 1985).

Orange luminescence of corundum is thus related to the presence of various F centers or their aggregates linked to a divalent cation - most likely Mg^{2+} – substituting for aluminium (Vigier et al., 2021). The formation of these small clusters of oxygen vacancies is relatively well-known and results from the agglomeration of simple vacancies in a range of temperature from 250 to 600 °C. To formulate this in a different way, some of these defects can be described as hole centers, the hole (the absence of an electron) being created by an oxygen vacancy with a global charge of -1 (instead of -2, as in O^{2-}). Note that for this emission there is no need to involve Fe^{3+} or Cr^{3+} with the hole center.

References

Atobe, K., Nishimoto, N., Nakagawa M., 1985. Irradiation-induced aggregate centers in single crystal Al2O3. Physica Status Solidi (a), 89-1, 155–162.

Vigier, M., 2021. Corundum: origin of orange luminescence (in French). Master's thesis. University of Nantes. 31 pages.

Vigier, M., Fritsch, E., Segura, O., 2021. Orange luminescence of corundum: an origin that is non-classical for gemmologists. First part (In French). Revue de Gemmologie AFG. n° 211, 12-19.

The Micro-World of Sapphire from Secondary Sources in Montana, USA

Nathan Renfro
GIA-Carlsbad CA, USA

There are three main commercial secondary deposits of sapphire from the state of Montana in the United States. In recent years, these sapphires have seen a surge in popularity and an increase in mining production, especially from the Rock Creek deposit. Other notable commercial deposits include the Missouri River and Dry Cottonwood Creek. Internal features among these three deposits are in many ways similar and the inclusions contained within these sapphires are distinctly different from the Yogo Sapphire deposit, which is a primary source of sapphire in Montana. These secondary sources often show hexagonal bands of rutile needles and particles, glassy melt inclusions, protogenetic rutile, metal sulfides and a number of other minerals. The surfaces of these sapphires also show that the rounded nature of the crystals is a result of resorption in the host melt and not mechanical abrasion as one might expect in stones transported to a secondary deposit.

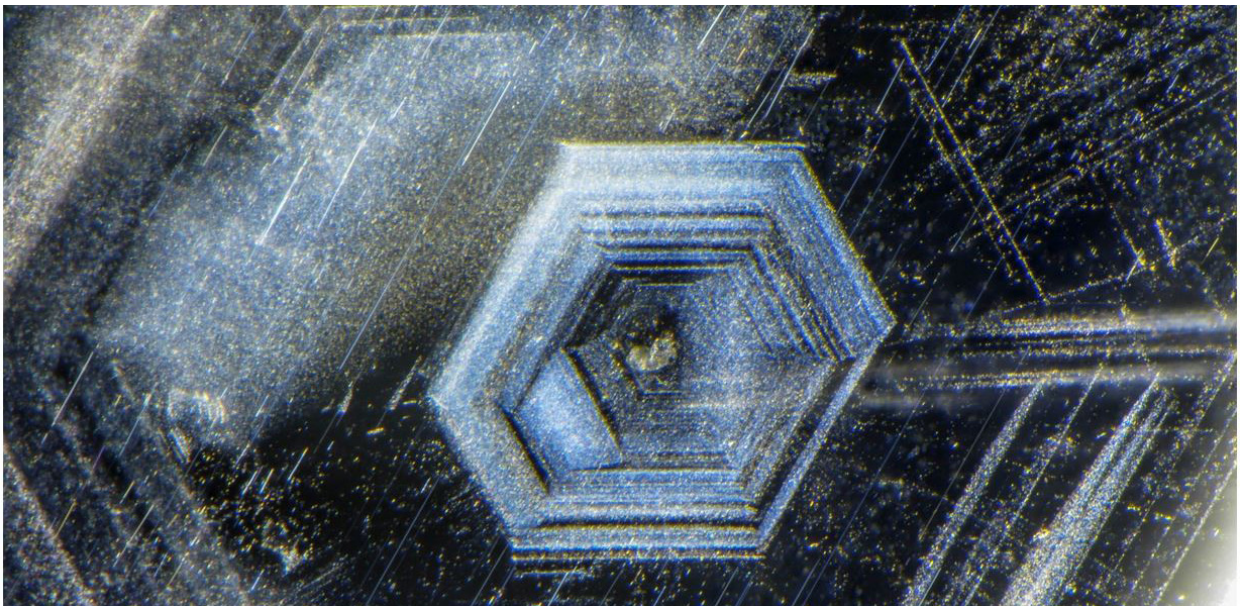

Hexagonal bands of dense rutile particles and needles may be found in all secondary sources of Montana Sapphire. Field of View: 3.31mm

The Fluorescence Characteristics and Identification of Copper Diffusion-Treated Red Feldspar

Qingchao Zhou[1, 2], Chengsi Wang[1], and Andy Hsitien Shen[1],*
1. Gemmological Institute, China University of Geosciences, Wuhan 430074, China
2. School of Jewelry, West Yunnan University of Applied Sciences, Tengchong 679100, China
(*communication author: shenxt@cug.edu.cn)

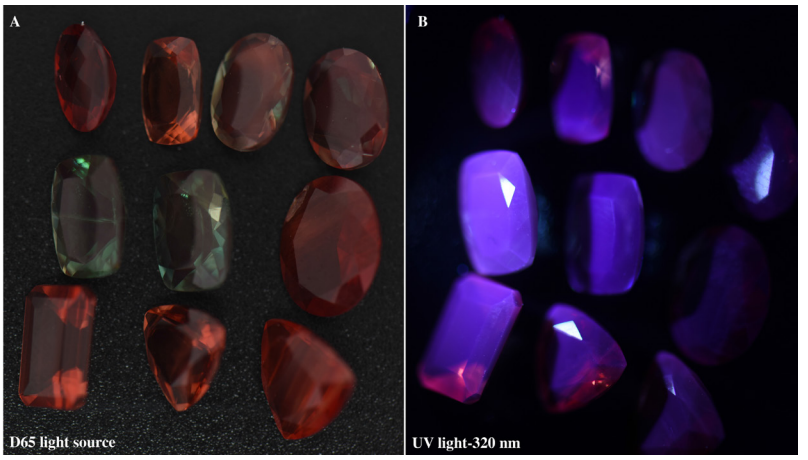

Figure 1. The appearance of commercial diffusion-treated red feldspar under D65 light (A) and UV light (B). Photo by Qingchao Zhou.

Natural sunstone from Oregon has been available for over a century. As the state stone of Oregon, this kind of rare and beautiful gemstone has a high market price. Owing to its high price and huge market potential, a kind of "new locality red feldspar" was unveiled at the Tucson Exhibition in the United States at the beginning of this century (Figure 1A). The gem sellers claimed that this kind of red feldspar came from a new locality, which attracted the attention of major gem research institutions around the world. Since the red feldspar and the natural Oregon sunstone have the same color origin, and the diffusion method of red feldspar on the market is still a mystery, many gemologists have made efforts to distinguish them from two aspects: gem identification technology (Rossman et al., 2011; Peretti et al., 2011;) and on-site inspection of the localities (Abduriyim et al., 2008; Abduriyim et al., 2009; Abduriyim et al., 2010). After nearly ten years of exploration, the current conclusion is that the reliability of this kind of "new locality red feldspar" is not high. Until now, there is still no convenient method that can quickly distinguish the natural sunstone from diffusion-treated red feldspar.

In this abstract, red feldspar samples were prepared in our laboratory through copper diffusion experiments. We want to understand the process and mechanism of copper diffusion treatment for feldspar first, and then find some evidence that can be applied to the identification. Just as we expected, we noticed that the diffusion-treated red feldspar samples appear typical fluorescence emissions near 394 nm and 555 nm compared with the nearly colorless feldspar roughs (Figure 1B). Based on this finding, the fluorescence spectra of natural sunstone samples from different localities and red feldspar samples from Tibet were systematically analyzed. The results show that fluorescence spectroscopy, as a non-destructive testing method, can be used to quickly distinguish the natural sunstone from diffusion-treated red feldspar. The details will be discussed in the presentation.

References

Abduriyim, A. (2008) Visit to andesine mines in Tibet and Inner Mongolia. Gems & Gemology, Vol. 44, No. 4, Winter, pp. 369–371.

Abduriyim, A. (2009) A Mine Trip to Tibet and Inner Mongolia: Gemological Study of Andesine Feldspar. GIA, News from Research. Sept. 10, 27 pp, http://www.gia.edu/ research- resources/news-from-research/andesine-mines-Tibet-Inner-Mongolia.pdf.

Abduriyim, A. (2009) The characteristics of red andesine from the Himalaya Highland, Tibet. Journal of Gemmology, Vol. 31, No. 5–8, pp. 283–298.

Abduriyim, A., Laurs, B.L. (2010) Andesine in Tibet: A second field study. InColor, No.15, Fall–Winter, pp. 62–63, http://icamedia.org/webincolor/FallWinter2010/index. html

Peretti A., Villa I., Bieri W., Hametner K., Dorta L., Fontaine G., Meier M., Günther D. (2011) Distinguishing natural Tibetan copper-bearing andesine from its diffusion-treated counterparts using advanced analytical methods. Contributions to Gemology, No. 10, pp. 1–105.

Rossman, G.R. (2011) The Chinese red feldspar controversy: Chronology of research through July 2009. Gems & Gemology, Vol. 47, No. 1, Spring, pp. 16–30.

Luminescence of gem topaz from Schneckenstein, Germany

Lutz Nasdala [1]*, Manuela Zeug [1], Chutimun Chanmuang N. [1], Christoph Hauzenberger [2], Manfred Wildner [1]

[1] Institut für Mineralogie und Kristallographie, Universität Wien, Althanstr. 14, 1090 Wien, Austria
[2] NAWI Graz Geozentrum, Karl-Franzens-Universität Graz, Universitätsplatz 2, 8010 Graz, Austria
***lutz.nasdala@univie.ac.at**

Yellow topaz unearthed at the world-famous Schneckenstein rock in Saxony certainly belongs to Europe's historically most important gems. Faceted stones are, among others, contained in historic jewellery that was manufactured in the 18th century during the reign of Friedrich August II (1696–1763), Elector of Saxony (and as August III also King of Poland and Grand Duke of Lithuania). Some of these jewels are now on display in the Green Vault, Dresden. The gemstones mostly have pale colour that is commonly described as "wine yellow" (Fig. 1). They are apparently inert under long- and short-wave UV lamps but show intense pinkish-red luminescence under violet (laser or LED) illumination. The phenomenon has been studied by excitation and emission spectroscopy and chemical analysis.

Figure 1. Hand-specimen from the Schneckenstein crag, exhibiting yellow topaz (large crystal is 2 cm tall) with quartz, on greisen. Photograph by Manfred Wildner.

The Schneckenstein topaz has a mean chemical composition corresponding to $Al_{1.99}Si_{1.01}O_{4.00}[F_{0.84}(OH)_{0.16}]_2$ and is generally low in non-formula elements (see also Breiter et al., 2013). Chromium (10–40 ppm) is too low in concentration to notably contribute to colouration. The Schneckenstein material therefore is not "imperial" topaz; its colouration is predominantly caused by defect-related "colour centres" (Petrov, 1977). It is well known that defect annealing upon thermal treatment may result in colour change of "imperial" and other topaz (Schott et al., 2003; Greenidge, 2018). For the Schneckenstein topaz, annealing causes nearly complete decolouration (Fig. 2), indicating that the absorption of Cr^{3+} and other transition metals is insignificant.

Figure 2. Three images of a Schneckenstein topaz crystal (6.5 mm longest dimension, 0.41 g). The natural yellow to pale brownish colour (left) appears fully bleached after dry annealing in air at 550 °C for 48 h (centre). Both the natural (not shown) and the annealed material (right) show fairly intense, pinkish luminescence under 390 nm LED illumination. Photographs by Manuela Zeug.

In topaz, Cr^{3+} causes readily visible emission when samples are excited with light in the 385–450 nm wavelength range (see again Fig. 2) whereas there is virtually no luminescence under long-wave UV light (~365 nm wavelength). This behaviour is similar to that of emerald but somewhat in contrast to ruby, which still shows vivid red luminescence under the long-wave UV lamp. The reason for differences in excitation characteristics between ruby and topaz is that slightly weaker crystal-field effects of topaz, compared to ruby, cause a shift of the main $^4T_1$ absorption band of Cr^{3+} to lower energies (that is, to longer wavelengths); the same is also true for other electronic levels (Fig. 3). For more details see the Tanabe-Sugano diagram for an ion with d^3 electronic configuration in octahedral coordination (Sugano et al., 1970).

The energetic downshift of the $^4T_2$ electronic level in topaz leads to virtual equilibrium between the ^2E level and the thermally populated $^4T_2$ level at room temperature (Gaft et al., 2003). The emission spectrum of topaz (see again Fig. 3) therefore consists of the spin-forbidden $^2E > {}^4A_2$ transition (two narrow R lines) and the spin-allowed $^4T_2 > {}^4A_2$ transition (underlying broad band). The latter is modulated by lower-intensity bands that were interpreted as emissions of pairs and clusters of Cr^{3+} ions (Gaft et al., 2003) and phonon satellites (Tarashchan et al., 2006), respectively.

The Schneckenstein topaz is certainly not unique, but perhaps somewhat special because this material shows fairly intense Cr^{3+}-related luminescence in spite of insignificant (in the sense of not causing colouration) Cr^{3+}-related absorption. The emission characteristics of "imperial" topaz with its much higher, colouration-affecting Cr content is quite similar to that of the Schneckenstein topaz. High emission intensity of the Schneckenstein material may in part be assigned to particularly low concentrations of luminescence "quenchers" such as Fe^{2+}. The majority of other pale gem topaz (Namibia, Pakistan, Ural) that we tested virtually did not luminesce at all.

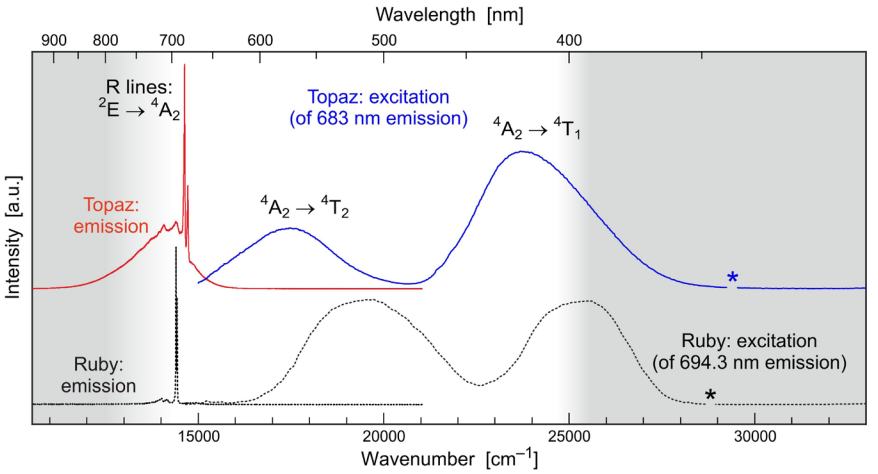

Figure 3. Excitation spectrum (i.e. intensity of the 683 nm Cr^{3+}-related emission in dependence of the excitation energy), and emission spectrum obtained using 473-nm laser excitation, of Schneckenstein topaz. Corresponding spectra of ruby are shown for comparison. Spectral ranges that are invisible to the human eye are underlain grey. Breaks in the excitation spectra, marked with asterisks, are analytical artefacts (twofold emission energy). Note the shift of the two main absorption bands between the two minerals. For band assignment see Tarashchan et al. (2006).

References:

Breiter, K., Gardenová, N., Vaculovič, T., Kanický, V., 2013. Topaz as an important host for Ge in granites and greisens. Mineralogical Magazine, 77(4), 403–417

Gaft, M., Nagli, L., Reisfeld, R., Panczer, G., Brestel, M., 2003. Time-resolved luminescence of Cr^{3+} in topaz $Al_2SiO_4(OH,F)2$. Journal of Luminescence, 102–103, 349–356

Greenidge, D., 2018. Investigations of color center phenomena in topaz and quartz through electron spin resonance with reference to optical absorption and nuclear magnetic resonance: Implications for extended mineral applications. Malaysian Journal of Fundamental and Applied Sciences, 2018,142–149

Petrov, I., 1977. Farbuntersuchungen an Topas. Neues Jahrbuch für Mineralogie, Abhandlungen, 130, 288–302

Schott, S., Rager, H., Schürmann, K., Taran, M., 2003. Spectroscopic study of natural gem quality "imperial"-topazes from Ouro Preto, Brazil. European Journal of Mineralogy, 15, 701–706

Sugano, S., Tanabe, Y., Kamimura, H., 1970. Multiplets of transition-metal ions in crystals. Academic Press, New York, London, 331 pp

Tarashchan, A.N., Taran, M.N., Rager, H., Iwanuch, W., 2006. Luminescence spectroscopic study of Cr^{3+} in Brazilian topazes from Ouro Preto. Physics and Chemistry of Minerals, 32, 679–690

Acknowledgements:

Thanks are due to Steffen Gerisch (Vogtländisch-böhmisches Mineralienzentrum Schneckenstein, Germany) for providing samples for analysis, Andreas Wagner for sample preparation, Gerald Giester for experimental help, and Wolfgang Zirbs (all Universität Wien, Austria) for acquiring literature. Comments by Michael Gaft (Ariel University, Israel) are gratefully acknowledged.

Colour mechanisms and heat treatment of blue Nigerian gahnites

Tom Stephan[1], Ulrich Henn[1] & Stefan Müller[2]

[1] German Gemmological Association, Idar-Oberstein
t.stephan@dgemg.com
[2] DSEF German Gem Lab, Idar-Oberstein

Among the minerals of the spinel group, the zinc end-member gahnite is found in gem-quality only sporadically. Besides green specimens from Brazil (Bank, 1975), green, blue, and green-blue material is known from an occurrence in Nigeria. This material originates from the Jemaa region in central Nigeria (Jacobson & Webb, 1946), and is associated to granitic pegmatites. A detailed gemmological description was published by Jackson (1982). In recent years, some lots of bright blue gahnite crystals from Nigeria were offered in the international gem trade (Boehm & Laurs, 2018, Hain & Sun, 2019) (Figure 1).

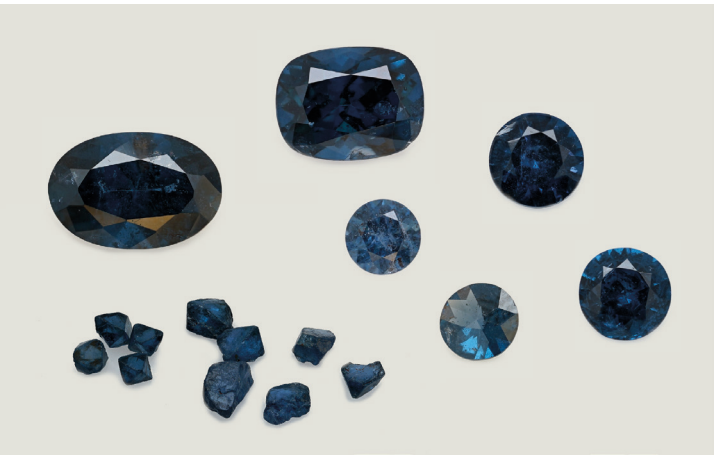

Figure 1. Bright to dark blue gahnites from Jemaa, Nigeria. The oval stone on the left weights 1.34 ct.

Jackson (1982) attributed the blue colour of the Nigerian gahnites to Fe^{2+}. Additionally, he mentions colour modifications from blue to blue-green and dark olive green by annealing after being heated to 1000 and 1400°C respectively. In detail, Fregola et al. (2014) described the absorption spectra of blue gahnite from Nigeria as a combination of Co^{2+}- and iron-bands.
For this study, a selection of blue gahnites from Jemaa/Nigeria has been investigated, both to show how strong Co^{2+} influences their colour and to explain the colour modifications from blue to green described by Jackson (1982).
The studied samples include 81 rough crystals sized from 3 to 6 mm in diameter. Additionally, 6 faceted samples were investigated weighing 0.22 to 1.34 ct. In comparison, various natural iron-bearing, and iron- plus cobalt-bearing spinels, as well as cobalt-bearing flux-grown synthetic spinels were examined.

Results & Discussion

For our Nigerian gahnite samples, the refractive index was determined ranging from 1.791 to 1.798 (measured with a digital refractometer, Presidium Refractive Index Meter II), with a specific gravity between 4.34 to 4.66. They were identified as relatively pure gahnites (approx. 91 mol.-% $ZnAl_2O_4$) by chemical analysis with a wavelength-dispersive electron microprobe (JEOL JXA 8200). An iron content of 2.90 to 3.18 wt.-% FeO was measured, which corresponds to a hercynite ($FeAl_2O_4$) component of approx. 8 mol.-%. Galaxite ($MnAl_2O_4$) and spinel s.s. ($MgAl_2O_4$) are present in contents less than 1 mol.-%. The cobalt content of the Nigerian material is 0.015 to 0.025 wt.-% CoO.

Optical absorption spectra were measured with a Perkin Elmer Lambda 950S UV/Vis/NIR-spectrometer in the spectral range between 200 to 2500 nm. The optical absorption spectra of the blue gahnites from Nigeria are dominated by three major band systems. The strongest system in the near-infrared region (approx. 1200 nm) is attributed to spin-allowed transitions of Fe^{2+} on tetrahedral coordinated structural sites (Taran et al., 2005). The strong absorption towards the UV and the UV-edge is caused by oxygen-metal charge-transfer processes (OMCT-bands) of $O^{2-} > Fe^{3+}$ and $O^{2-} > Fe^{2+}$ (Taran et al., 2005).

Between these two systems weaker bands are found in the visible and nearest infrared region. This band system is caused by a combination of mostly spin-forbidden, but also spin-allowed transitions of the chromophores Fe^{2+}, Co^{2+} and Fe^{3+}. In combination, their strongly overlapping absorption bands create a transmission window in the blue spectral region. To distinguish them, however, is difficult.

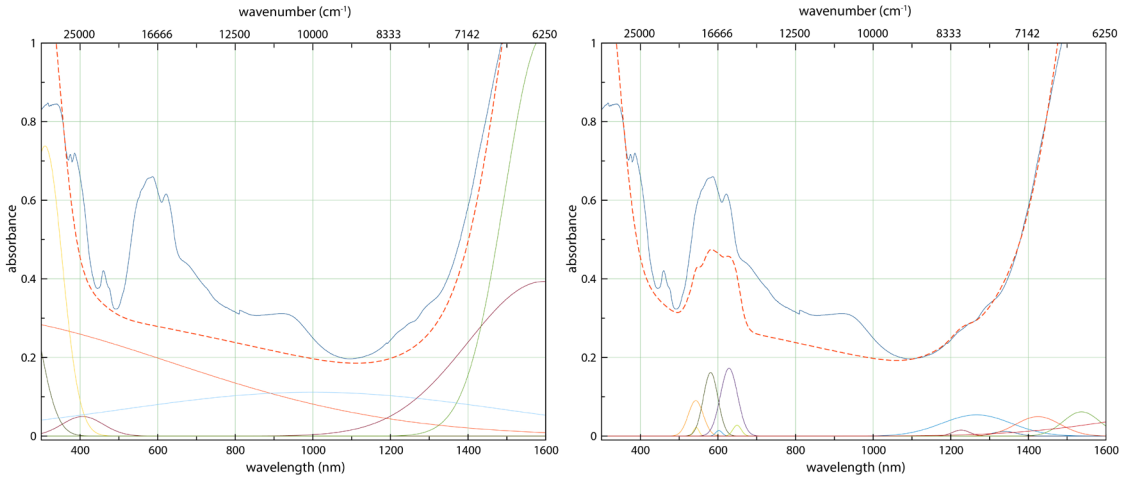

Figure 2. The absorption spectrum of a Fe-Co-bearing blue gahnite from Nigeria (blue trace) with underlying spectral fitting curves. On the left, the background has been modelled. On the right, the influence of cobalt is shown.

To demonstrate the influence of Co^{2+} the absorption spectra of the described gahnites were mathematically decomposed by spectral fitting, using the non-linear curve fitting software *MagicPlot*. For this purpose, the spectra of flux synthetic spinels coloured only by Co^{2+} were used to develop a model, which then was used to calculate the influence of Co^{2+} on the colour of the Nigerian gahnites (see Figure 2).

Finally, two of the rough crystals were heat treated to explain the colour modifications described by Jackson (1982). In the first step they have been heated for one hour in oxidizing conditions at 1000°C, in a second step for one hour at 1400°C. After the first step, the samples became darker greyish blue with a slightly greenish hue, after the second step they became dark blueish-green. These colour modifications can be explained by a stronger influence of Fe^{3+}, which is most likely created during heat treatment (see Figure 3). On one side, the Fe^{3+}-bands in the visible range became stronger. More important, however, are the stronger Fe^{3+}-O^{2+}-charge transfer bands (OMCT-bands) towards the UV, causing a stronger absorption of the blue and violet light, shifting the transmission window towards the green spectral region.

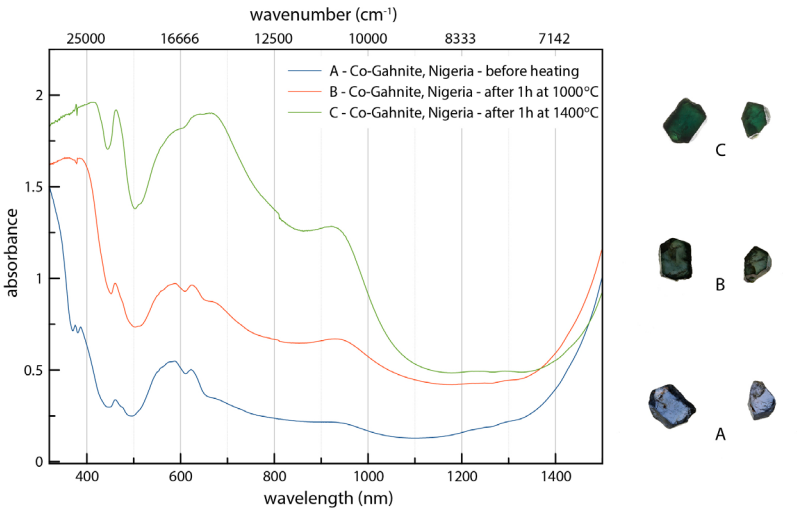

Figure 3. The two gahnites from Nigeria on the right have been heated at different temperatures. The corresponding absorption spectra of the larger sample are shown on the left.

This new production of blue Fe- and Co-bearing gahnite from Nigeria proves to be an interesting addition to the trade and for gemstone collectors. These blue gahnites usually are cut in rather small size, due to the size of the rough, but also as they tend to become very dark and included and thus less attractive when cut to larger size.

References

Bank, H., 1975. Durchsichtiger grüner Gahnit aus Brasilien. Z. Dt. Gemmol. Ges. 24, 90-91 (in German).
Boehm, E. and Laurs, B., 2018. Blue Gahnite from Nigeria. J. Gemm. 36 (2), 96-97.
Fregola, R. A., Skogby, H., Bosi, F., D`Ippolito, V., Andreozzi, G. B. and Halenius, U., 2014. Optical absorption spectroscopy study of the cause for color variations in natural Fe-bearing gahnite: Insights from iron valency and site distribution data. American Mineralogist 99, 2187-2195.
Hain, M. and Sun, Z., 2019. Blue Gahnite from Nigeria. Gems & Gemol. 55 (3), 434-436.
Jackson, B., 1982. Gem quality gahnite from Nigeria. J. Gemm. 18 (4), 265-276.
Jacobson, R. and Webb, J.S., 1946. The Pegmatites of Central Nigeria. Geological Survey of Nigeria Bulletin No. 17.
Taran, M. N., Koch-Müller, M. and Langer, K., 2005. Electronic absorption spectroscopy of natural (Fe2+, Fe3+)-bearing spinels of spinel s.s.-hercynite and gahnite-hercynite solid solutions at different temperatures and high-pressures. Physics and Chemistry of Minerals, 32 (3), 175-188.

Acknowledgements

The sample material has been kindly loaned and partly donated by the companies HC Arnoldi e.K., Kirschweiler, Germany and Gemstore24, Herrsching am Ammersee, Germany. The chemical analysis has been carried out by Dr. Stephan Buhre of the working group petrology of the institute for Geoscience at the Johannes Gutenberg-University in Mainz, Germany.

The colouring agent of pink jadeite

Masaki Furuya

Japan Germany Gemmological Laboratory, Kofu, Japan; jggl@sapphire.co.jp

Keywords: Pink jadeite, Myanmar, Manganese colouration

Beside the highly reputed green colour, jadeite can be found in various further colours, such as white, gray, black, blue, lavender (light to medium violet), yellow and reddish orange (only in heated stones). In 2009, 9 pink jadeite samples reportedly from Myanmar were obtained at a gem show in Hong Kong. They consist of three ring-shaped plates and six cabochons (Fig.1).

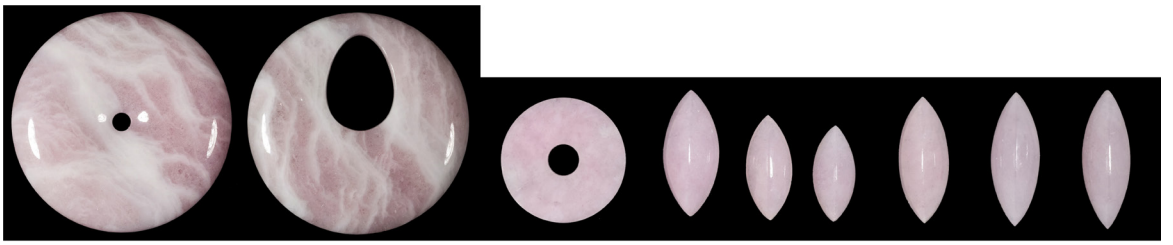

Figure 1. 9 pieces of pink jadeite samples and their major diameter

The colour of pink jadeite in the recent market is mostly either "false" (created by a pink string) or due to a treatment. The "false" coloured pink jadeite usually occurs as beads strung on a vivid pink thread. Though they are actually translucent white jadeite, they simply transmit the colour of the vivid pink string and pretend to look pink (Fig. 2 & 3).

The colour of treated pink jadeite is derived from impregnated pink resin. Such treated pink jadeite sometimes has colour strains and often reveals a strong orange fluorescence under long-wave UV light (Fig.4). And with FTIR, it shows a series of strong absorption peaks related to artificial resin at 2967, 2928, 2872, 3124, 3098, 3056 and 3037 cm^{-1}. In the UV-Visible absorption spectrum, such treated pink jadeites are characterized by two broad absorption bands centered at about 517 and 545nm due to the artificial colour pigment.

Figure 2. False pink jadeite beads

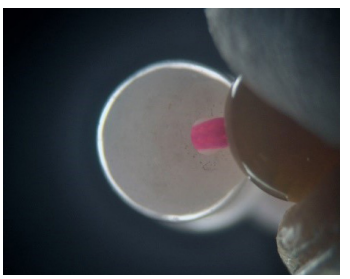

Figure 3. The translucent white jadeite and vivid pink string inside

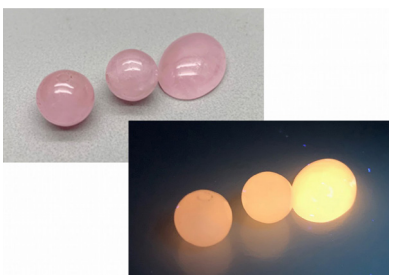

Figure 4. The pink resin impregnated jadeite and its fluorescence under LWUV

In contrast to this, the 9 pink jadeite samples investigated for this study did not show any features of treatment mentioned above, thus seem to be naturally coloured. For the 6 cabochons, the pink colour is almost homogeneous, whereas the plate samples show white veins in a pink body colour. And one of the plate samples has a small green part also. With microscopic magnification, the fibrous structure of jadeite can be seen, but no colour stain is found in all samples. With long-wave UV light, some of them show small spots of orange-red fluorescence which can be seen also in lavender jadeite.

The FT-IR spectra of these pink jadeite samples also did not show any indications of treatment except tiny peaks related to wax, a traditional surface "enhancement" applied to most jadeites. With UV-visible spectrometer, all samples show a characteristic broad absorption band at about 540 nm. Their peak position varies a little from 535 to 555 nm. Also, all samples show a 437 nm peak due to Fe^{3+} as known from many other jadeites. (Fig.6)

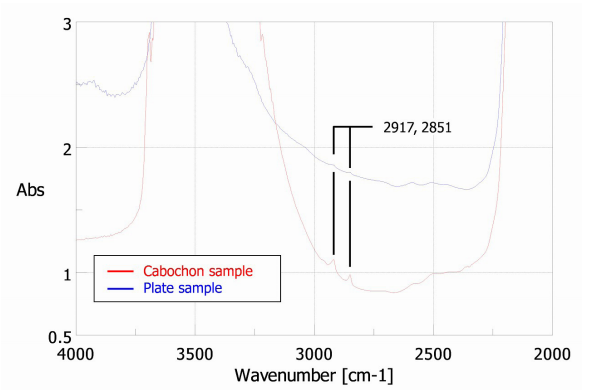

Figure 5. FT-IR spectrum of pink jadeite reveals small peaks related to wax in a cabochon sample and even less visible wax peaks in the plate sample.

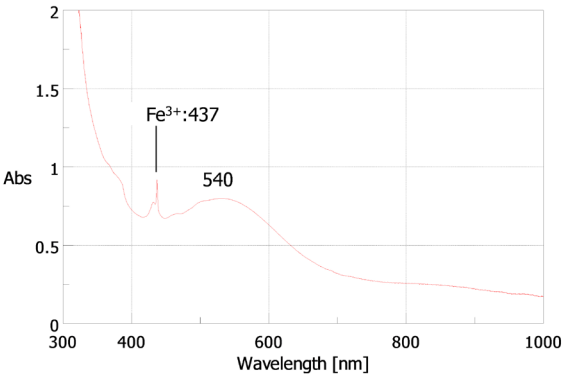

Figure 6. UV-Vis spectrum of pink jadeite showing a broad absorption band at about 540 nm related to the presence of manganese (responsible for the pink colour) and a distinct Fe^{3+} peak.

The colouration of lavender jadeite is commonly explained by using the pink to purple pyroxene member spodumene as analogy, as it has a crystal structure similar to jadeite (Lu 2012). In the case of pink to purple spodumene, manganese is considered the colouring agent which causes the absorption band centered at 540 nm (Lu 2012). It is similar to the pink jadeite in this research. LA-ICP-MS analyses carried out on one of the plate samples at the pink body part and at the white vein part reveal that the manganese content is higher at pink part up to 260 ppm and quite low as 2-12 ppm in the white vein (Fig. 7). In contrast to this, other potential colouring elements such as titanium, iron, vanadium and chromium are almost equal in both colour parts. Thus, the main colouration of pink jadeite is confirmed to be manganese as Lu suggested using the analogy of spodumene.

At the same time, the difference between lavender and pink jadeite can be described by iron and titanium contents. The scatter plots of Figure 7 and 8 compare the trace elements content of lavender, gray (dull lavender), pink and white vein part of pink jadeite. As shown in Figure 7, the manganese content in lavender and pink jadeite are almost same. About the iron and titanium, the lavender jadeite has higher content for both of them than pink and white vein part of pink jadeite. From these features of trace elements, it can be said that manganese is responsible for pink colour and iron and titanium add the blue or violet tint to it to cause the so-called lavender colour.

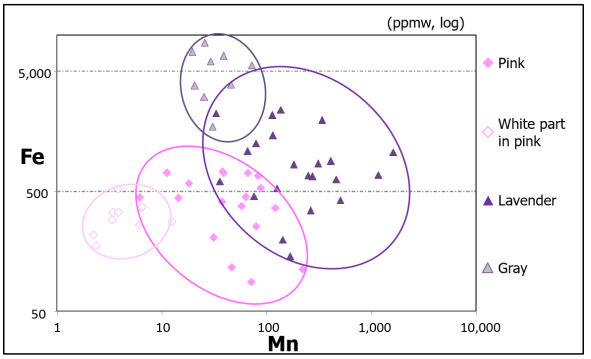

Figure 7. Mn and Fe content in jadeite

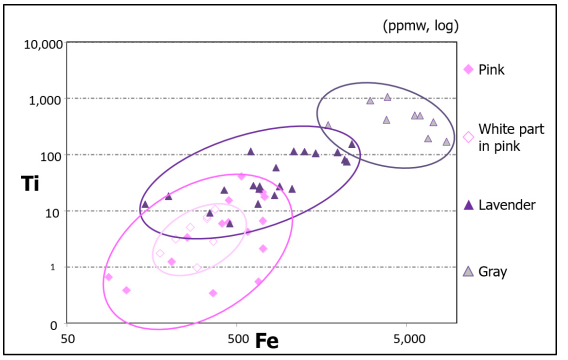

Figure 8. Fe and Ti content in jadeite

In this research, it was confirmed that manganese is the main colouring agent in pink and lavender jadeite of natural colour. And the difference of colour between lavender (purple to violet) and pink jadeite is supposed to be related to a higher iron and titanium content in lavender jadeite, causing a bluish to violet tint in these stones.

Acknowledgments
Aya Nakajima
Yamanashi Prefectural Industrial Technology Center

References

R. Lu (2012) Color origin of lavender jadeite, Gems and Gemology 48(4):273-283

Comparative characteristics of gem-quality diaspore from Afghanistan and Myanmar

Claudio C. Milisenda[1], Michael Wild[2]
[1]DSEF German Gem Lab, Prof.-Schlossmacher-Str. 1, D-55743 Idar-Oberstein, Germany, gemlab@dgemg.com
[2]Werner Wild oHG, Hauptstr. 474, D-55743 Idar-Oberstein, info@wild-edelsteine.de

The mineral diaspore is well known to gemmologists as an inclusion in corundum. When present, it strongly suggest that its host did not experience any heat treatment. Gem-quality diaspore is known from the Mugla Province in Turkey (Schmetzer & Bartelke, 1979). They commonly show a colour change from brownish-green hues in daylight to pinkish hues in incandescent light. These diaspore varieties become more commonly known in the beginning of this century when larger quantities were marketed under the trade names „Zultanite" and „Csarite", respectively. Recently transparent, purplish-pink diaspore reportedly from a new source in Afghanistan appeared on the market (Nicastro et al., 2020).

Figure 1. Faceted and rough diaspore from Afghanistan

We had the opportunity to examine both rough and faceted material reportedly from the same new source near the village of Ragha in the Nangarhar Province of eastern Afghanistan and compare it with purple to purple-red diaspore from Myanmar (Burma). Burmese gem-quality diaspore was first described by Kyi & Win in 2004.

Samples from Afghanistan are shown in Figure 1. The rough material weighed between 0.3 and 0.7 grams and two faceted stones tested had a weight of 1.26 ct. and 4.43 ct., respectively.
Cut specimens of several tens of carats have been reported (Smith et al., 2020). In fact, we have certified a faceted stone of almost 100 ct.

The crystals show a distinct trichroism with purplish-pink, yellow and pink colours. The refractive indices of the faceted stones were $n\alpha = 1.700$, $n\beta = 1.724$ and $n\gamma = 1.749$ with a maximum birefringence of $\Delta n = 0.049$. The thin tabular crystals from Burma were also strongly pleochroic and showed a distinct colour zoning. The weight of the samples shown in Figure 2 ranged from 0.07 to 0.2 grams. The refractive indices of a faceted stone were consistent with those of diaspore from Afghanistan.

Figure 2. Rough diaspore from Myanmar

UV/VIS/NIR spectra showed absorption bands which correspond to those of trivalent chromium, vanadium and iron. Chemical analysis using EDXRF spectrometry showed chromium concentrations of less than 0.06 % Cr_2O_3 for Afghan diaspore whereas the specimens from Myanmar showed elevated chromium contents of up to 1.20 wt.% Cr_2O_3. The contrasting chromium contents can also be deduced from different photoluminescence spectra. In addition, Burmese samples tend to have higher vanadium and lower iron concentrations when compared to specimens from Afghanistan. Data sampling is still in progress, however the physico-chemical characteristics allow a clear separation between diaspore from Afghanistan and diaspore from Myanmar.

References

Kyi, U.H., Win, K.K., 2004. A new deposit of gem quality colour-change diaspore from Möng Hsu, Myanmar. Australian Gemmologist, 22(4), 169–170.

Nicastro, I., Vertriest, W., Renfro, N., Sun, Z., Palke A., Mattlin, P., 2020. Purplish pink diaspore reportedly from Afghanistan. Gems & Gemology 56(2), 298-301.

Schmetzer, K., Bartelke, W., 1979. Schleifwürdiger Diaspor aus der Türkei. Z.Dt. Gemmol. Ges. 28(2), 69.

Smith, M.H., Lhuaamporn, T., Laurs, B.M., 2020. Pink diaspore from Afghanistan. J. Gemmol. 37(3), 240-242.

Cu-containing Thin Sheet Inclusion in Cu-bearing Tourmaline from Brazil

Hao A.O. Wang[1], Daniel Grolimund[2], Leander Franz[3], Daniel Mathys[4], Rainer Schultz-Güttler[5], Michael S. Krzemnicki[1]

1 Swiss Gemmological Institute SSEF, Basel, Switzerland. (hao.wang@ssef.ch)
2 MicroXAS Beamline, Swiss Light Source, Paul Scherrer Institute, Switzerland.
3 Dept. of Environmental Sciences, Mineralogy and Petrology, Universität Basel, Switzerland.
4 Nano Imaging Lab, Swiss Nanoscience Institute, Universität Basel, Switzerland.
5 Institute of Geosciences, University of São Paulo, Brazil.

Cu-bearing tourmaline was first discovered in 1987 in granitic pegmatites in Paraíba state in Brazil. It immediately became one of the most sought-after tourmaline species in the gem trade, thanks to its attractive vivid blue (to green) colour, also described as "neon" or "electric" blue. Depending on its chemical composition, Cu-bearing tourmaline can be found in a range of colours, from blue to green to even purple and pink.
Our study focusses on a green Cu-bearing tourmaline sample (Fig. 1) from Brazil, containing oriented metallic-looking thin sheet inclusions. This rarely-seen inclusion has been reported previously in a few studies (Fritsch et al. 1990, Brandstätter et al. 1994, Hartley 2018) and was suggested to be native Cu and tenorite (CuO) formed during epigenetic exsolution (Koivula et al 1992).

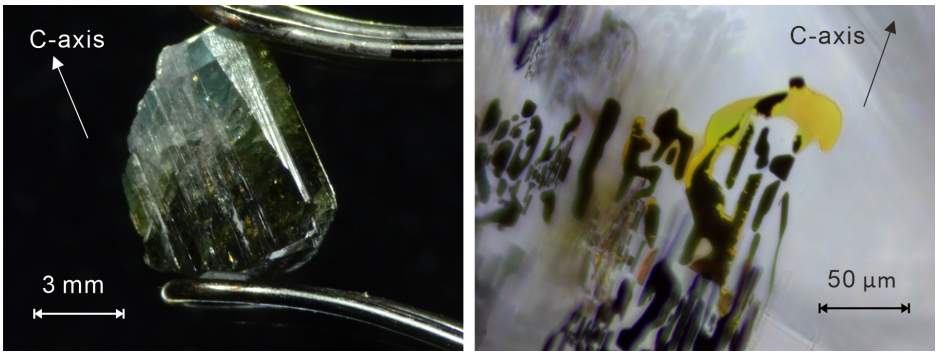

Figure 1. Left: Cu-bearing tourmaline from Brazil containing a rare type of highly reflective inclusions investigated in this study. Crystal width is about 5 mm. Right: Microphoto of the thin sheet inclusion in transmitted light, revealing two clearly separated phases (black and yellow).

In our sample, the inclusion planes are aligned parallel to the C axis direction of the host tourmaline. We used a focused ion beam (FIB) in combination with scanning electron microscope (SEM) to cut the sample and image the cross-section of the inclusion. Detailed SEM pictures showed that the inclusion is about 150 nm in thickness (Fig. 2). A chemical profile across the cross-section was carried out by energy dispersive spectroscopy (SEM-EDS). In the profile, the Cu signal increased at the position of the inclusion, while no elevated S signal was observed. In contrast to Brandstätter & Niedermayr (1994), in our sample we did not see an obvious decrease of Cu in the tourmaline host on each side of this thin sheet inclusion.

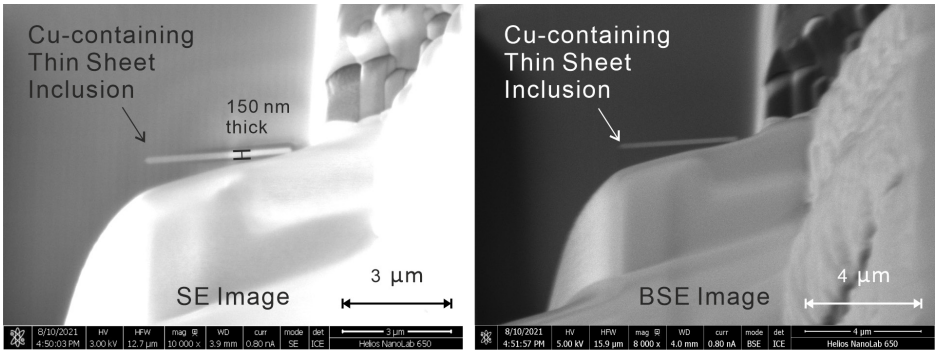

Figure 2. Left: Secondary electron image (SE) of a thin sheet inclusion in Cu-bearing tourmaline revealing a thickness of about 150 nm. Right: Backscattered electron image (BSE) of the same inclusion showing brighter color than the host tourmaline, indicating the presence of high Z elements in the inclusion compared to the tourmaline host.

Using micro-FTIR, we noticed a small shift in the OH absorption peak positions (around 3000-4000 cm^{-1}) in the thin sheet inclusion region compared to the nearby tourmaline host. Raman spectra showed extra peaks in the tourmaline host in the inclusion region than in the tourmaline host further away from the inclusion, which may indicate species of tourmaline other than elbaite being present near the thin-sheet inclusion. Subsequently, we focused on investigation of the inclusion by spatially resolved Synchrotron Radiation X-ray absorption spectroscopy (XAS). The result showed that Cu is probably present as a metal phase (zero oxidation state) in the thin sheet inclusion.

Based on our preliminary observation, the Cu-containing thin sheet inclusions are probably Cu metal. Nevertheless, the hypothesis that these inclusions form due to epigenetic exsolution from the Cu-bearing tourmaline host is in debate. Definitely, more analyses are required to better understand the nature and formation of these inclusions. The outcome may provide crucial information on the oxidation conditions during the formation of Cu-bearing tourmaline from Brazil.

References

Brandstätter, F., and Niedermayr G., 1994 - Copper and Tenorite Inclusions in Cuprian-Elbaite Tourmaline from Paraiba, Brazil. Gems & Gemology, 30 (3): 178–183.

Fritsch, E., Shigley J.E., Rossman G.R., Mercer M.E., Muhlmeister S.M., and Moon M., 1990 - Gem-Quality Cuprian-Elbaite Tourmalines From São José Da Batalha, Paraíba, Brazil. Gems & Gemology, 26 (3): 189–205.

Hartley, A., 2018 – Native Copper Inclusions in a Cu-bearing Tourmaline. Journal of Gemmology, 36 (3): 203.

Koivula, J.I., Kammerling R.C., and Fritsch E., 1992 - Tourmaline with Distinctive Inclusions. Gems & Gemology, 28 (3): 204.

Trapiche-Skeleton Quartz from Inner Mongolia: Crystal Morphology, Internal Features and Possible Formation

Shang I (Edward) Liu[1], Pornsawat Wathanakul[2]

[1] The Gemmological Association of Hong Kong, Hong Kong; gemedward@hotmail.com
[2] Department of Earth Science, Kasetart University, Thailand; pwathanakul2@gmail.com

Keywords: Trapiche quartz, crystal morphology, formation

Quartz crystal samples and some trapiche cut products were collected from Huanggang Fe-Sn skarn deposit, East Ujimqin Banner, Inner Mongolia Autonomous Region, China (Fig. 1).

(a) (b)

Figure 1. (a) Huanggang Fe-Sn skarn deposit; (b) Trapiche cut products

Crystal Morphology

From specimens inspected, the morphology of quartz crystals can be grouped into three categories (Frondel 1962; Kantor 2003) as follows:

Type I: Cathedral morphology normally shows hexagonal prismatic crystals, which are usually 8-12cm long, 3-4 cm wide (Fig. 2). Exceptional large crystals may be up to 30cm in length. The euhedral crystals are milky and sub-translucent to opaque with lateral overgrowth formation of protruded crystal edges and depressed prism faces, suggesting that the edges and corner grew faster than the prism faces themselves due to uneven crystallization (Sunagawa 2007). When cut into slices (perpendicular to the c-axis) and polished, they show an obvious trapiche skeleton with a fixed light brownish, translucent six-rayed star trapiche pattern, showing dendritic arms from the centre to the edges of the hexagonal prismatic faces. These translucent arms show relatively less inclusions. Microscopically, a lot of fibres (probably hollow tubes) were found in radiated pattern which were distributed in six sub-translucent to opaque triangular sectors between the arms. Disturbances in the crystal growth by tiny fluid blebs and/or impurities are suspected to be the cause of those fibres. Hematite detected by Raman spectroscopy occurs as inclusions and as secondary reddish staining around the crystal rim.

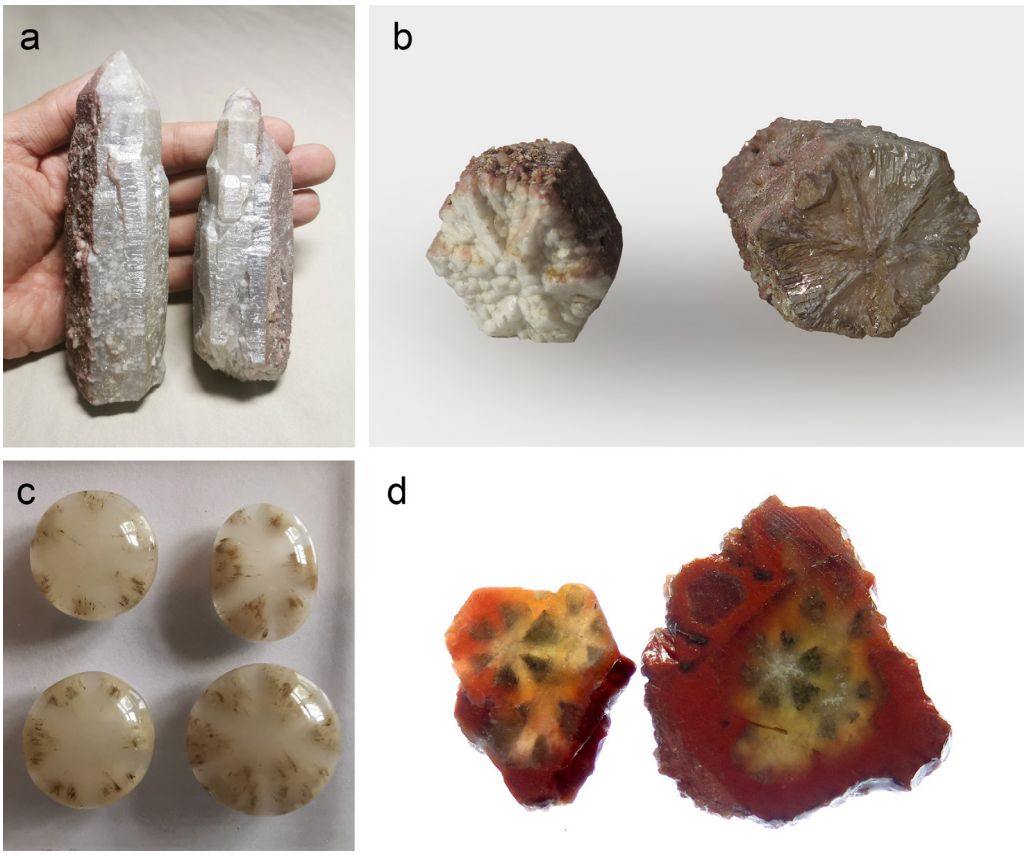

Figure 2. (a) Cathedral type of quartz crystal samples (left: 12.2x3.8 cm; right: 10.6x3.4 cm); (b) both showing a protruded trapiche growth pattern at one termination of quartz crystal; (c) Some cabochon cut products of this type of quartz; (d) Two slices shows multi trapiche pattern with reddish staining rim

Type II: Tessin morphology occurs in long and thin, sub-transparent to translucent crystals, around 7-13cm long, and 2-3cm wide, with a green, red or yellow, sub-translucent to opaque core and six milky, occasionally brownish, triangular sectors containing fibrous inclusions extending radially to the depressed center of the prism faces (Fig. 3a). This type of trapiche quartz usually exhibits "Tessin" habit (named after the Swiss Kanton Ticino/Tessin) with the hexagonal prism getting continuously thinner (alternating steep r rhombohedral faces and m prism faces) towards the tip of the crystal. After cutting the crystal into slices (perpendicular to the c-axis), the trapiche growth pattern becomes obvious and the slices near the crystal termination are relatively clean and transparent (Fig. 3b). They show interference colours and a trapiche growth pattern under cross-polarized light (Fig. 3(c)- top), similar to trapiche quartz from Colombia (Krzemnicki & Laurs, 2014). The slices coming from the middle part of the prismatic crystal display the same morphology as the Type-1 trapiche quartz. They show a six-sectored trapiche pattern containing radiating fibres (usually milky in colour) starting from the centre of the crystal and oriented perpendicular or nearly perpendicular to the rhombohedral crystal faces. The slices from the base of this trapiche quartz are characterised by having a greenish and sub-translucent pseudo-hexagonal core, which shows another trapiche pattern with six dark green arms (or more transparent arms) going from the centre to the edges of the core. The combined use of Raman spectroscopy and XRF indicated that the green to brownish green fibrous inclusions can be chlorite, hedenbergite or grunerite (Farfan 2021). Red and yellow mineral associations are hematite (Fritch 2001) and an unknown fibrous clay mineral (Fig. 4).

(a) (b) (c)

Figure 3. (a) This Tessin type quartz crystal (6x2cm) shows the distribution of inclusions under transmitted light; (b) Nine cut and polished slices of the quartz crystal (perpendicular to the c-axis), show the trapiche growth pattern and transparency changing at different parts of the crystal; (c) Three selected slices show different patterns under cross-polarised light.

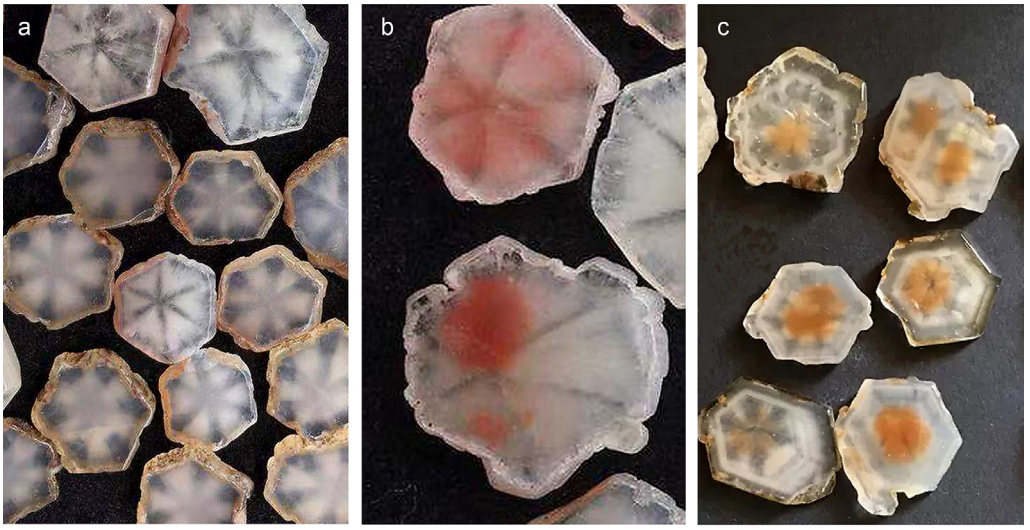

Figure 4. (a) Relatively clean slices cut from Type-2 trapiche quartz crystals; (b, c) The red and yellow colours are caused by mineral inclusions identified as haematite and an unknown fibrous clay mine respectively.

Type III: Artichoke morphology appears in long sheaf-like crystals, around 10-20 cm in length and 2.5-7 cm in width) (Fig. 5a). This kind of sprouting quartz was called artichoke quartz after a report by Rykart (1995). It is a special splitting growth of quartz with many sub-individuals diverging from the main crystal. Such overgrowths cover the hexagonal prism faces and horizontal striations that are common in a quartz crystal, and make it look relatively round when viewing parallel to the c-axis. Most of them are doubly terminated; few of them may show a long trunk at the other end. Although this type of trapiche quartz crystals do not exhibit a clear skeletal growth pattern, they are characterised by having special tips of star-shape edges between the rhombohedral faces standing out from the crystals. When cutting, the trapiche growth pattern can only be found in the part of "artichoke" termination where the epitaxial lateral growth occurred. Intense fibres/cavities are seen between the arms, but also sometimes surrounding the outer rim of the crystal. These fibres are oriented in radiating pattern perpendicular to the morphologically dominant rhombohedron faces.

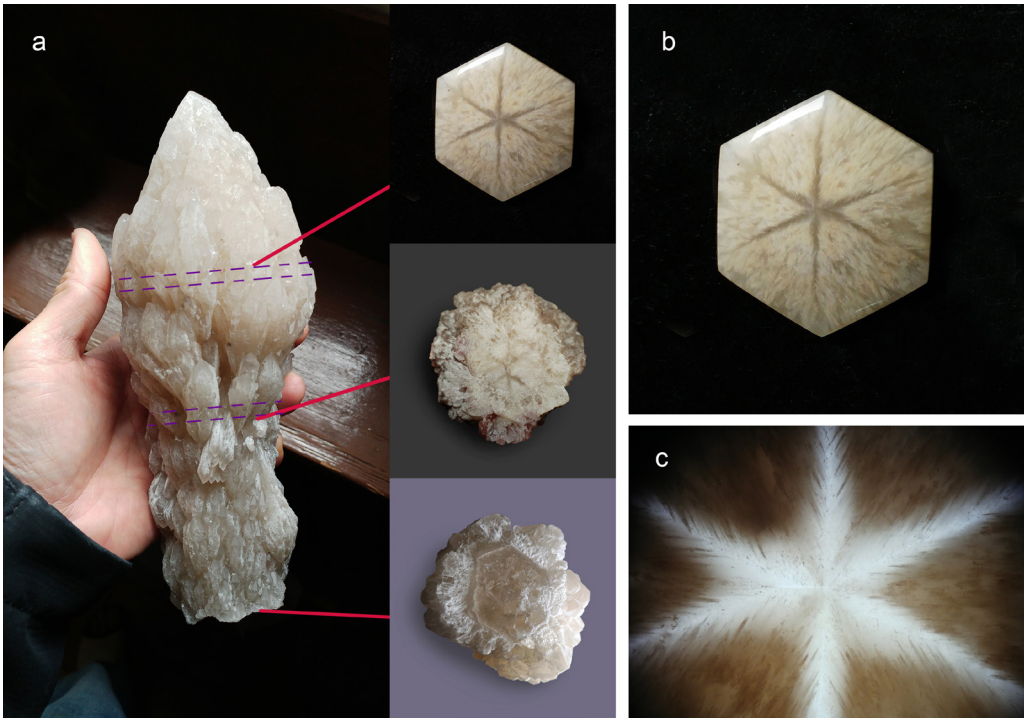

Figure 5. (a) Artichoke type of quartz crystal sample (7x17cm) and its cross-sections (viewed parallel to the c-axis); (b) a hexagonal single cabochon cut product from this type of quartz; (c) intense radiating fibres between the arms, under magnification.

Possible formation

According to the crystal morphology, internal features of growth structure (zoning) and mineral association, it is suggested that those trapiche-skeleton quartz samples from Inner Mongolia likely formed under multiple growth mechanisms at different stages of crystallisation (Takahashi et al. 2004). The late state hydrothermal fluid must be enriched in silica, iron oxide impurities and clay minerals. The Type I of Cathedral morphology shows the early state of relatively pure dendritic arm formation allowing the later quick formation of trapezoidal growth sectors under pneumatolytic conditions, including some impurities. Some crystals may have the overgrown formation of silica and iron oxides with associated layers of hematite and limonite. The multi-trapiche skeleton morphology of Type II would have more supply of silica in the ambience when forming quick six dendritic arms with different growth rates,

providing the quartz twinning formation on the prism faces on the longer arms as substrates for growing, leading to the multi-connected trapiche-skeleton crystal growth of quartz. The iron oxides may also play an important role as the impurities triggered quartz crystallisation of this type. The red colour is due to alteration products of secondary iron minerals. The Type III of Artichoke-like morphology shows trapiche-skeleton formation that likely differs from the other two types. The internal features reveal that the impurities would first trigger the quartz crystallisation from the crystal centre and be squeezed out by crystallisation crosscutting through the prisms of the crystal, with possible impure inclusions and fluid blebs resulting in the trapiche patterns like those usually appear in some blue sapphires from some localities (Wathanakul 2004).

Acknowledgements
The authors are grateful to Tsui Kin Wah Tommy, Lau Chun Kit and Li Sheung Yin Timothy of China Gems Laboratory Limited for providing Raman spectroscopy, FTIR spectroscopy and EDXRF experiments.

References
Emmanual F., 2021. Hematite Inclusions in Red Trapiche Quartz from Inner Mongolia. The Journal of Gemmology. Gem Notes, 37(6), 569-571.
Farfan G.A., Rakovan J, Ackerson M, et al. 2021. The origin of trapiche-like inclusion patterns in quartz from Inner Mongolia, China. American Mineralogist, 2021-7454 (in press).
Frondel C., 1962. The System of Mineralogy of J.D. Dana. III. Silica Minerals (Seventh Edition). John Wiley, New York and London, 334 pp.
Kantor B.Z., 2003. Crystal Growth & Development: Interpreted from a Mineral's Present Form. Ocean Pictures Ltd., Moscow, Russia, Mineralogical Almanac, Vol.6, 128 pp.
Krzemnicki M., Laurs B., 2014. Quartz with Radiating Fibres, Sold as 'Trapiche' Quartz. The Journal of Gemmology. Gem Notes, 34(4), 296-298.
Sunagawa I., 2007 Crystals: Growth, Morphology, & Perfection. Cambridge University Press. Cambridge, UK, 295 pp.
Takahashi Y., Imai H., Hosaka M. et al. 2004. Epitaxial Lateral Overgrowth (ELO): The mechanism of formation of scepter, skeletal, cathedral and related quartz morphologies. European Journal of Mineralogy, 16(6), 1009-1017
Wathanakul, P., Atichat, W., Pisutha-Arnond, V. et al. 2004. Evidences on the unusually high Be, Sn, Nb and Ta content in some trapiche-like sapphires from basaltic origins. 29th International Gemmological Conference, Wuhan, China, September 12-21, 2004. 114-118.

Persian Turquoise
A review on the current state of Neyshabur turquoise mine, Iran

Bahareh Shirdam[1], Andy H. Shen[1], Yang Mingxing[1], Zahra Mokhtari[2], Hamed Fazliani[3]

shirdam@gmail.com
[1] Gemological Institute, China University of Geosciences, Wuhan, 430074, China
[2] Department of Geology, Faculty of Science, University of Neyshabur, Neyshabur, Iran
[3] Neyshabur Turquoise Mine Co-operative, Neyshabur, Iran

Located in the Razavi Khorasan Province of northeastern Iran, 53 km from the city of Neyshabur, the Neyshabur mine has produced the majority of Iranian turquoise for more than a millennium. Yet in recent decades there have been claims that the mine is on the verge of closure, that its turquoise quality has diminished, or that it is running out of resource. Such claims often carry enormous weight with consumers. After visiting the Neyshabur turquoise mine in 2020, a report was conducted on the current state of the mine that is in fact quite active and still expanding.

The mine is located at Raish Mountain, where turquoise has been recovered for millennia. Today the Neyshabur turquoise mine consists of three active tunnels: Main, Dom, and Zahk. Each will be discussed separately.

Among Iran's main three turquoise deposits, only the Neyshabur mine is dedicated to turquoise production. Baghu turquoise is from the Kuh Zar mine, a gold and copper deposit, and Shahr-I Babak turquoise comes from the Meiduk mine, a porphyry copper deposit. The mining strategies at Kuh Zar and Meiduk are focused on the extraction of gold and copper, respectively, rather than turquoise. Despite the fine color of Baghu turquoise, the Kuh Zar mine currently reports no official production of turquoise. On the other hand, the Meiduk open-pit mine is working with the Shahr-I Babak turquoise co-operative to manage the turquoise extracted in the process of copper mining. Open-pit mining has caused an unstable turquoise yield. When there is a turquoise vein on one of the horizontal levels known as benches, the mine can produce an average of three tons per month, but otherwise there could be no production for months. More information on the Kuh Zar and Meiduk mines will be published in subsequent reports.
With more than 200 workers, an average production of four tons of rough turquoise per month, and an annual production of 40 to 42 tons, Neyshabur is Iran's largest turquoise mine.

The rough turquoise quality extracted from the mine is divided into four main categories; Turquoise nuggets and slabs (Figure 1A), Turquoise with the host rock attached (Figure1B), Chalky turquoise (Figure1C), Turquoise chips (Figure 1D).

[1]The tunnel's original Persian name "Asli" literally translates to "Main."

Figure 1. The four major quality levels of rough turquoise production from Neyshabur: turquoise nuggets (A), turquoise with the host rock attached (B), chalky turquoise (C), and turquoise chips (D). Photos by B. Shirdam.

New giant gem corundum boulder from Sri Lanka

Thanong Leelawathanasuk[1], Supparat Promwongnan[1], Pornsawat Wathanakul[2], Visut Pisutha-Arnond[1], Wilawan Atichat[1] and Gamini Zoysa[3*]

[1]The Gem and Jewelry Institute of Thailand, Bangkok, Thailand
[2]The Gems and Mineral Sciences Special Research Unit, Department of Earth Science, Faculty of Science, Kasetsart University, Bangkok, Thailand
[3*]Sri Lanka; gaminizoysa3@gmail.com

Abstract

Recently, a very large water-worn boulder of corundum aggregate (100x75x50 cm, 510 kg) was found near the village Kahawatta, situated about 28 km southeast of Ratnapura (Figure 1). The specimen was mined at a depth around 15-18 meters below the surface in an alluvial gem mine. Kahawatta is a well-known gem mining area which has produced several large sapphires previously. One of the biggest stones was a 43 kg single corundum crystal found in 1995 (Gunaratna and Dissanayake, 1995).

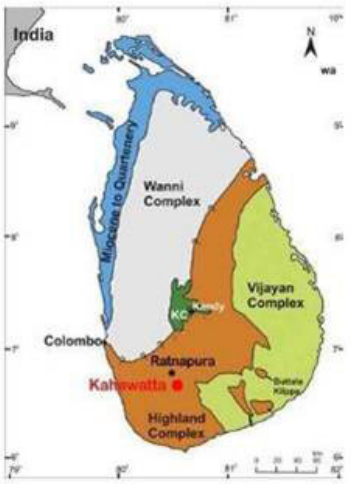

Figure 1.Geological map of Sri Lanka showing the location of Kahawatta mining area where the giant corundum boulder was found. The area is situated in the Highland Complex. Map modified afterCooray(1984).

The mining area belongs to the Highland Complex of Sri Lanka which consists predominantly of quartzite, dolomitic marble and calcsilicate gneiss (and quartzitic schists). The country rocks exposed near the mining area are granulite and garnet gneiss.

The boulder is composed mainly of interlocking euhedral to subhedral crystals of corundum with various sizes ranging from 0.5 to 6 cm. Other interstitial minerals were completely dissolved out which appear as voids.

A few crystals extracted from the boulder were cut as cabochon by the owner; they display a good asterism. Some crystals fragments were also heat-treated by traditional methods to enhance their colour and clarity. Two samples (untreated and heated) were selected to analyse their gemmological properties at the GIT laboratory in Bangkok (Figure 2).

Gemmologicalproperties

The untreated sample is an irregular-shaped rough (97.71 ct, 31.6 x 23.8 mm), exhibiting milky and very light grayish blue colour, whereas the heated sample is a polished piece (8.00 ct, 14.5 x 11.8 mm) showing medium blue colour (Figure 2 right).

The untreated sample showed an RI of 1.76 (distance vision technique), and the heated and polished sample an RI of 1.760-1.770 (birefringence = -0.010). The specific gravity (SG) values of both samples was 3.98-4.02. These values fall well within the range of corundum. The untreated sample was inert under long- and short-wave UV, while the heated samples showed a strong chalky under short-wave UV, but was inert to long-wave UV-light

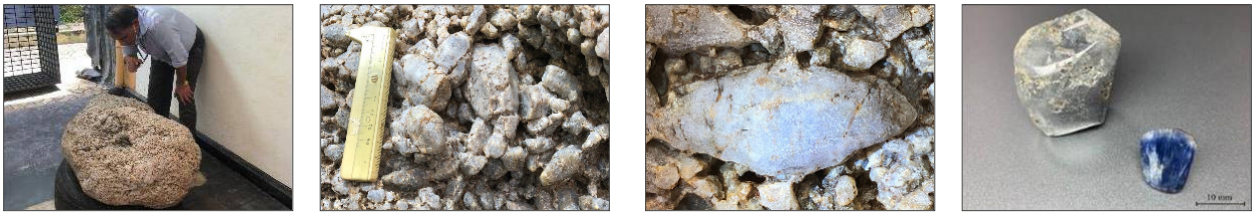

Figure 2. A: The described large water-worn boulder of corundum aggregate (100x75x50 cm, 510 kg) from the Kahawatta mining area, Ratnapura, Sri Lanka. B: Interlocking euhedral to subhedral corundum crystals and interstitial voids. C: Close up of euhedralcorundum crystals approximately 5 cm long. D: An untreated, milky, and very light greyish blue sapphire rough (97.71ct, upper left) and a heated and polished blue sapphire piece (8.00ct, lower right) from that boulder which were analyzed gemmologically at GIT Thailand.

The internal features found in the untreated sample were fingerprints, minute particles, and dark crystals which were identified as uraninite by Raman spectroscopy. In addition, very dense regularly orientated needle-like inclusions intersecting at approximately 60°/120° were identified as rutile. These needles are responsible for the star effect when cut properly as cabochon. The heated stone showed uneven colour zoning, fingerprints, melted crystals, and tube-like inclusions. Growth zone of this sample was obviously seen as fluorescence image under Diamond View.

UV-Vis-NIR Absorption Spectra

The non-polarized UV-Vis-NIR absorption spectrum of the treated (blue) sample showed a distinct absorption band at about 580 nm related to Fe^{2+}/Ti^{4+} Intervalence Charge Transfer (IVCT). This is typical for blue sapphire of metamorphic origin. The untreated sample, however, revealed a similar but much weaker Fe^{2+}/Ti^{4+} IVCT absorption band compared to the heated blue sample. The strong blue body coloration of the heated sample is likely to be due to the dissolution of minute (rutile) particles connected with a "bleeding" (internal diffusion) of the titanium from the rutile needles into the host lattice of corundum.

Chemical composition

Semi-quantitative chemical analyses by EDXRF of the untreated sample gave Fe_2O_3 0.12 wt%, Cr_2O_3 0.01 wt%, V_2O_3 0.02 wt%, TiO_2 0.05 wt%, and Ga_2O_3 up to 0.02 wt%. The heated stone showed rather similar amount of trace elements, except a higher titanium concentration (TiO_2 0.12 wt%). Concludingly, the chemical analyses match very well with the GIT database of sapphire samples from Sri Lanka.

Conclusions

Lithologically, the large boulder recently discovered is indeed a water-worn corundum aggregate of rather poor gem quality. It is however possible to cut some grayish star sapphires out of this material. The acid drop testing showed effusive bubbles, indicating the probable presence of some carbonate matrix. Uraninite and rutile inclusions are not enough for a detailed interpretation of the geological origin of the corundum boulder, possibly it is of metamorphicand/or pegmatoid-related origins. Further advanced analyses may provide more information. Based on the observed surface condition, we assume that the described boulder of corundum aggregate was found close to its primary host rock. Consequently, the nearby alluvial deposits could be an area of interest for prospection to find further material to be cut into this type of star sapphires. The analyzed and presented data can be used as representative characteristics of the Kahawatta star sapphires from Sri Lanka.

References:

Cooray, P.G., 1984. An introduction to the geology of Sri Lanka (Ceylon), 38. National museums of Sri Lanka publication.

Gunaratna, H.S and Dissanayake, C.B., 1995. Gem & Gem Deposit in Sri Lanka.

Myanmar Gold-Lipped Cultured Pearls

By Tay Thye Sun, Thet Tin Nyunt, Myo Lwin, Tay Zar Linn, Gina Brombach, and Michael S. Krzemnicki

Abstract
Cultured pearls from Myanmar are famous for their silver and golden colour and also its valuable mother-of-pearl shells. An ideal place for pearl cultivation was found many years ago at Pa Lel Kyun island (formerly known as Sir J. Malcolm island) (Fig.1), Myeik (or Mergui) Archipelago in the Andaman Sea off southern Myanmar. The Myanmar pearl-farming industry started in 1954 as a joint venture between Burma Pearl Fishing and Culture Syndicate and the Japanese pearl farmer Kichiro Takashima, under the name South Sea Pearl Co. The industry has since expanded to about 14 jointventure companies with operations that spread across various islands off Myeik Archipelago. The estimated size of Myanmar Pearl Enterprise (MPE) company farming at the Pa Lel Kyun is about 8 km (5 miles) surrounding the island to about 13 km (~7.8 miles).

Figure 1. The Pa Lel Kyun island (formerly known as Sir J. Malcolm island) is where Myanmar golden lipped cultured pearl began in 1954. (Photo by Tay Thye Sun)

The mollusc used for pearl cultivation is Pinctada maxima. Besides collecting wild spat from the surrounding islands, MPE has hatchery stations since 1980s. In 1998 they established a modern hatchery station on the island to supplement for the growing spat production which is in use until today. A temperature-controlled room kept at 20°C is used for cultivating phytoplankton to feed the spat. The spats grow in tanks where they hang on strings for about 28 days, with about 200 spats on each string and 96-160 strings in each tank. After the spat has grown to about 12 mm size (after about 60 days), they are transferred to small frames surrounded by netting, with each frame holding only 12 spats to encourage their growth. The frames are suspended in the ocean for approximately two months and then the spats are transferred to new frames. After 18 months, the oysters reach about 12 cm in size. At this age, a bead nucleus of 4.5-7.0 mm size is implanted in the gonads of each oyster. Afterwards, the oyster are placed in panel nets and returned to the ocean for two years.

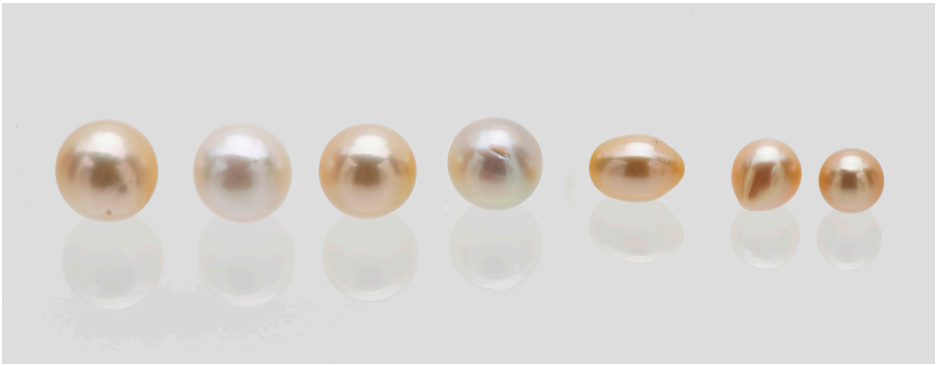

Figure 2. The shape of Myanmar golden lipped cultured pearl from round to off rounded, size range from 14 mm to 9 mm (from left to right) with colours range from yellow to light yellow and slightly creamy. (photo by Michael Krzemnicki)

The author (TTS) bought seven cultured pearls (Fig.2) from a pearl supplier at Myeik for further research. The size of our samples ranges from 9 to 14 mm, and their colour from yellow, light yellow to slightly cream. Our analyses confirmed that they are beaded cultured pearls from the gold-lipped pearl oyster (Pinctada maxima). Chemical analyses (EDXRF) revealed a composition typical for saltwater (cultured) pearls with only low traces of manganese (Mn). In radiography and X-ray microtomography, all samples exhibit a spherical bead with a nacre overgrowth which varies considerably in thickness from 0.5 mm to 3 mm with an average of about 2 mm. UV-Vis-NIR reflectance spectra are similar to those described by Elen (2001) for untreated pearls from Pinctada maxima. More data about these attractive cultured pearls from Myanmar will be published soon by the authors.

Acknowledgement:
Many thanks to travelling companion Nyi Nyi Aung and also to Win Thein (assistant general manager) and Sai Aye Cho (marine biologist) and the staff of MPE's pearl farm Pa Lel Kyun, and also much appreciation to SSEF for conducting the pearl analyses.

References:

Domingo B.S., 2020. Myanmar eyes solid footing in global pearl market. Jewellery Net: Market Intelligence news 3th February 2020. https://www.jewellerynet.com/en/jnanews/features/23683

Elen S., 2001. Spectral reflectance and fluorescence characteristics of natural-color and heat-treated "golden" South Sea cultured pearls. Gems & Gemology, Vol. 37, No. 2, 114-123.

Strack, E., 2006. Pearls. Ruhle-Diebener Verlag, Germany, 707 pages.

Sze Man Young, 2018. Myanmar pearl dealer eyes Asia. JNA, 46.

Sze Man Young, 2019. Myanmar finds footing in global pearl sector. Pearl Report, 36.

Tay Thye Sun, Thet Tin Nyunt, Myo Lwin, Tay Zar Linn, 2021. Visit to a gold-lipped cultured pearl farm in Myanmar. Journal of Gemmology, Vol.37, No.5, 463-464.

Tint Tun, 1998. Myanmar Pearling: past, present and future. In: SPC Pearl Oyster Information Bulletin, No. 12, 3-7.

Progress in studying pigment evolution during the growth of freshwater cultured pearl

Chaoyang Chen[a#] Yaping Xiong[b#] Yijiang Hong[b*] Andy H Shen[a*]

a. Gemmological Institue, China University of Geoscience (Wuhan), Wuhan 430074, China;
b. School of Life Sciences, Nanchang University, Nanchang 330031, China
# These authors contribute equally to this abstract and should be considered as co-first author
* Co-corresponding author

Pearl is an organic gemstone and the color is an important factor determining the quality of pearl, so the pigments in pearls are concerned by gemologists. The pigments in freshwater pearls (Unionidae) are considered to be carotenoids and/or polyene pigments with various carbon-double-bond chain lengths (Heedegard et al. 2006, Karampelas et al. 2007, Karampelas et al. 2020). Previous studies mainly focus on the pigment of pearls after complete growth, we hope to research the evolution of pearls pigment at different growth stages. We grew freshwater pearls with Hyriopsis cumingii and Hyriopsis schlegelii mollusks using and sampled the resulting cultured pearls every 30 days for a total of 90 days. We implanted a live tissue fragment prepared from the mantle of a donor pearl mollusk into the mantle of a recipient pearl mollusk together on top of a small inorganic flat disc made from shell of mollusk (instead of a spherical bead). Raman spectroscopy is used to characterize the pigments in pearls. We collected Raman spectra of pearls with different growth times (30 days and 60 days) and we also simulated the theoretical Raman spectra of polyenes with different carbon-double-bond chain lengths using Density Functional Theory (DFT) based quantum chemical simulation software. According to comparing experimental and theoretical Raman spectra, we speculate that the chain length of polyene pigment may change during the growth of pearl. Further characterization of the pearls with longer growth period (90 days) and high-performance liquid chromatography-mass spectrometer (HPLC-MS) analyses are currently ongoing in our Lab.

Keywords: Freshwater cultured pearl; Polyene pigment; Raman spectra; DFT calculation.

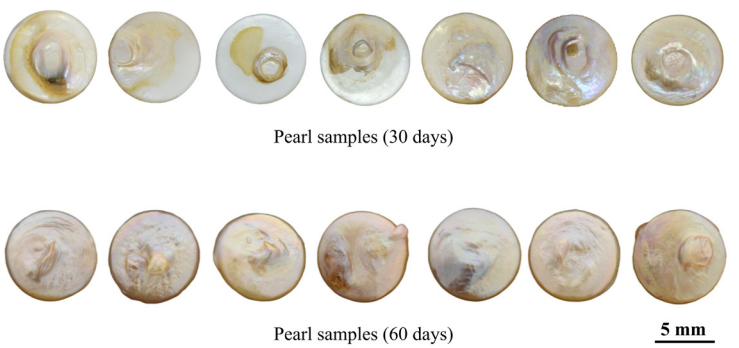

Figure 1. Pearl samples cultured for 30 days and 60 days using a flat disc as "bead"

References

Hedegaard C., Bardeau J-F., and Chateigner D. (2006). Molluscan shell pigments: an in-situ resonance Raman study. Journal of Molluscan Studies, 72, 157-162.

Karampelas S., Fritsch E., Mevellec J.-Y., Gauthier J.-P., Sklavounos S., and Soldatos T. (2007). Determination by Raman scattering of the nature of pigments in cultured freshwater pearls from the mollusk Hyriopsis cumingi. Journal of Raman Spectroscopy, 38 (2), 217-230.

Karampelas S., Fritsch E., Makhlooq F., Mohamed F., and Al-Alawi A. (2020). Raman spectroscopy of natural and cultured pearls and pearl producing mollusc shells. Journal of Raman Spectroscopy, 51 (9), 1813-1821.

Analysis of Japanese Akoya Cultured Pearls using LA-ICP-MS

Kentaro Emori*, Hiroshi Kitawaki (Central Gem Laboratory),
Masahiro Sato, Junko Yazaki (Pearl Science Laboratory)
*Corresponding author: emori@cgl.co.jp
Keywords: Akoya Cultured Pearl, LA-ICP-MS

In recent years, Akoya cultured pearls are cultured not only in Japan but also in China, Vietnam, UAE and so on. Japanese Akoya cultured pearls are popular as a JAPAN BRAND, and the origin determination of Japanese Akoya cultured pearls has commercial significance as traceability which is sometimes topic for other gem stones, and study on the difference among farms is also interesting in science.

However, the determination is not simple. Pearls are taken from the mother mollusks and processed every year. Since chemicals are used for processing, protein components in the nacre may be dissolved away or the chemicals may be deposited. In addition, the chemical composition of the sea area to be cultured may not be uniform even in one area, and the concentrations of trace elements vary year by year.

In this study, we measured concentrations of trace elements of pearls by LA-ICP-MS, collected from various stages of processing and from different farms, in order to discuss the possibility of origin determination of pearls.

Influence of the processing on trace elements should be investigated using pearls produced in one farm, but it was not possible to collect the pearls from one farm. Instead, we collected 20 Akoya cultured pearls farmed in three places, Tsushima, Iki and Sasebo, in Nagasaki Prefecture, and the 20 samples for analysis are classified as follows; 5 unprocessed pearls, 5 pearls pretreated overnight at 50°C with methanol (pretreated pearls), 5 pearls bleached 1 to 6 weeks with 2% hydrogen peroxide solution after pretreatment (bleached pearls), 5 pearls were toned overnight using a 0.1% dyeing solution after bleaching (dyed pearls).

In order to investigate the difference among farms, we analyzed each 10 pearls farmed in 2021 from the 6 farming areas; Shima in Mie Prefecture, Komobuchi in Ehime Prefecture, Amakusa in Kumamoto Prefecture and Iki, Tsushima and Sasebo in Nagasaki Prefecture (figure 1).

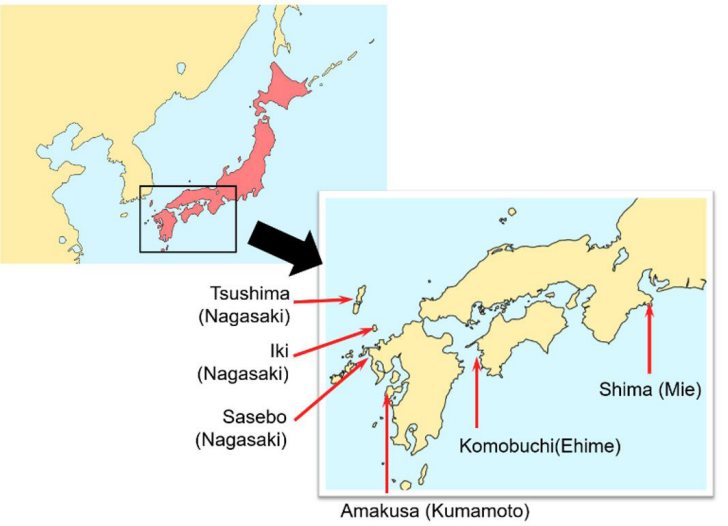

Figure 1. Pearl farming area studied in this study

We used a LA-ICP-MS apparatus, consisting of NWR UP-213 as Laser ablation and Agilent 7900rb as ICP-MS.
As a result, some differences were observed in concentrations of B, Na, Mg, K, Mn and Sr from pearls in each stage of processing, but they were within the error range, and it was not possible to conclude definite influence of the processing on trace elements.
Regarding the pearls from the 6 farming areas that were farmed in 2021, it was found that the pearls from Shima, Mie Prefecture, had more Mn than the other production areas, and those from the production areas in Nagasaki Prefecture had less Mg than the others (figure 2). In addition, sorting using the algorithm of principal component analysis (PCA) has revealed clear distinction between pearls from the four prefectures of Mie, Ehime, Kumamoto and Nagasaki Prefecture (figure 3), although it is difficult to distinguish the three production areas in Nagasaki Prefecture (Iki, Tsushima, Sasebo).

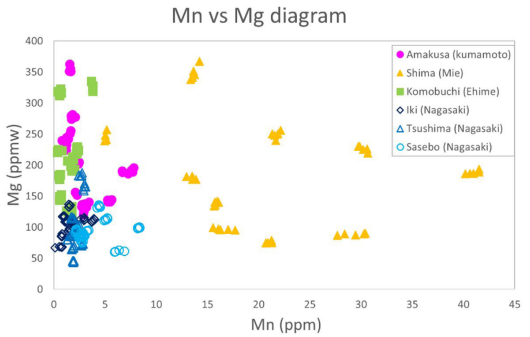

Figure 2. Mn vs. Mg diagram of pearls from 6 farming areas

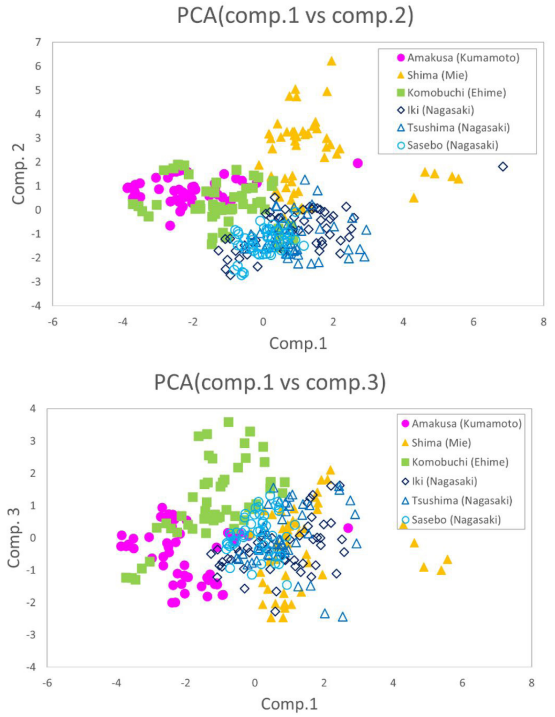

Figure 3. PCA of data of pearls from 6 farming areas. PCA (comp. 1 vs comp. 2) shows difference between Nagasaki Prefecture and other prefectures. PCA (comp. 1 vs comp. 3) shows difference among Kumamoto, Mie and Ehime Prefectures

Regarding the identification of pearl farming area using LA-ICP-MS, it has been found that some trace elements are different in pearls farmed in the four prefectures, and it is expected that analysis of trace elements is available for origin determination of pearls, although we have to consider many factors related to the farms.